Chapter 8

The Superconducting Order Parameter in High-Tc Superconductors – A Point-Contact Spectroscopy Viewpoint

M. Tortello and D. Daghero

Additional information is available at the end of the chapter

http://dx.doi.org/10.5772/59587

1. Introduction

Superconductivity can be regarded as a macroscopic quantum phenomenon. In quantum mechanics, particles can be described as wavefunctions with an amplitude and a phase. The striking effect occurring in the superconducting state is that electrons couple together forming Cooper pairs which can all be described by the same wavefunction, the order parameter (OP). In some cases, a superconductor can feature multiple order parameters but still preserving its macroscopic quantum nature.

High-temperature superconductivity (HTSC) was discovered in 1986 in copper-based compounds (cuprates) by J.G. Bednorz and K.A. Müller [1], who were awarded the Nobel prize the following year. Cuprates have now been extensively studied, but a definitive answer concerning the fundamental mechanism responsible for the occurrence of their superconducting state has not been given yet [2].

A report in February 2008 of superconductivity in the Fe-based compound $LaFeAsO_{1-x}F_x$ with a critical temperature $T_c = 26$ K [3], soon increased up to 55 K in similar compounds [4], raised exceptional interest in the whole solid-state-physics community. One of the reasons for this excitement was that a new class of high-temperature superconductors based on Fe instead of Cu was discovered. It is hoped that the study of this new class might clarify the other and, ideally, HTSC in general.

This discovery is certainly the most important in the field in the past 26 years. Many papers have been published on this topic: in October 2010, about 2000 experimental and 500 theoretical papers were already published and/or posted on the arXiv, an online repository for electronic preprints of scientific papers. Considerable progress has been achieved in a relatively short

time, but several crucial points are still awaiting definitive proof, and some apparently contradicting results still have to be reconciled.

In this regard, the knowledge of the number, amplitude and symmetry of the order parameters in a superconductor is a fundamental building block of any microscopic theory of superconductivity and therefore is mandatory in order to fully understand the physics of high- T_c superconductors. Moreover in the most complete theories of superconductivity, like the Eliashberg theory, the order parameter can be dependent on energy giving the possibility, in some cases, to experimentally resolve features related to the electron-boson interaction that is the fundamental glue producing the electron pairing and the emergence of superconductivity. This is very important as the knowledge of the microscopic mechanism responsible for the occurrence of superconductivity can help searching for new superconductors with higher T_c and better properties, in view of their application.

In this chapter we will briefly summarize (with no claim of exhaustiveness) the most relevant aspects of high-temperature superconductors that have been investigated by point-contact spectroscopy, mainly (but not only) in the regime of Andreev reflection. In section 2 we will introduce the very basic concept of order parameter, and provide an overview of the symmetries that have been proposed for various high-temperature superconductors. Section 3 will describe the technique of point-contact spectroscopy, the conditions that must be fulfilled in order to obtain reliable spectra, and the mechanism of Andreev reflection. The models used to describe this mechanism and to fit the experimental spectra (in order to extract information about the number, the amplitude and symmetry of the gap(s)) will be discussed as well.

Section 4 will finally provide a quick overview of the main results of point-contact spectroscopy in the two major classes of high-temperature superconductors, namely the cuprates and the iron-based compounds. It will be shown how the capabilities of point-contact spectroscopy have been extended and the relevant models have been refined in order to face the challenge represented by these very complex materials.

2. The Superconducting Order Parameter (OP)

The first successful (semi-)microscopic [5] theory of superconductivity was the Bardeen-Cooper-Schrieffer (BCS) theory [6, 7]. In the BCS picture, an attractive interaction between electrons (no matter how weak) can generate an instability of the Fermi sea towards the formation of pairs of electrons (Cooper pairs). The coupling is strongly favored for electrons with opposite spin and momentum. In conventional superconductors this interaction is rationalized as being due to the exchange of a virtual phonon between two electrons. However, the theory itself does not require specifying what is the origin of the attractive interaction and can thus be generalized to describe any kind of pairing glue other than that caused by phonons. Since the BCS ground state turns out to be favorable in energy with respect to the Fermi sea ground state, at $T=0$ all electrons are paired and, as already noted, they are described by a single wavefunction, the order parameter. In order to create single quasi-particle states, Cooper pairs have to be "broken apart" by giving to the system an energy equal to 2Δ, where Δ is the

http://dx.doi.org/10.5772/59587

energy gap that separates the BCS ground state from the lowest-lying single-particle excitations. Δcorresponds to the amplitude of the order parameter. The meaning of its name is clear because it indicates that there are no allowed quasi-particle states at energies between $E_F - \Delta$ and $E_F + \Delta$.

In the original BCS paper [6] the theory is formulated in a weak electron-phonon coupling approximation. Therefore, it is assumed that the energy gap is much smaller than the typical phonon energy, $\Delta \ll k_B\theta_D$(θ_D being the Debye temperature).

In this way, the electron-phonon pairing V, which would in general be dependent on the wavevector $\boldsymbol{k}$, can be approximated as $V_{\boldsymbol{k},\boldsymbol{k}'} = -V$ (BCS approximation) for energies below $k_B\theta_D$ and zero elsewhere. The minus sign indicates that the potential is attractive. Within this approximation the expression for the temperature-dependent energy gap is

$$\Delta(T) = 2NV\int_0^{k_B\theta_D} d\epsilon \frac{\Delta(T)}{2\sqrt{\epsilon^2 + \Delta(T)^2}} \tanh\left[\frac{\sqrt{\epsilon^2 + \Delta(T)^2}}{2k_BT}\right] \quad (1)$$

where N is the electronic density of states at the Fermi level for a definite spin and NV is the BCS coupling parameter. The equation can be solved numerically. The gap is therefore constant and isotropic over the whole Fermi surface and it is usually said that in this case the symmetry of the order parameter is of the isotropic s -wave type, i.e. $\Delta(\boldsymbol{k})=\Delta_0$(see Figure 1).

2.1. The anisotropy of the OP, multiple OPs and some important symmetries

If the pairing potential $V_{\boldsymbol{k},\boldsymbol{k}'}$ is no longer assumed to be constant over the Fermi surface (FS), the original BCS formulation can be generalized[1] and the expression for the gap becomes [8]

$$\Delta(\mathbf{k},T) = \int V(\mathbf{k},\mathbf{k}')\Delta(\mathbf{k}',T)\left[\int_0^{k_B\theta_D} \frac{d\epsilon}{\sqrt{\epsilon^2 + \Delta(\mathbf{k}',T)^2}} \tanh\left(\frac{\sqrt{\epsilon^2 + \Delta(\mathbf{k}',T)^2}}{2k_BT}\right)\right] dN' \quad (2)$$

where $dN' = dS'/4\pi^3\hbar v_F'$ is the element of the density of states associated with the area dS' of the Fermi surface and where the summation over $\boldsymbol{k}'$ implies also summation over all bands crossing the Fermi level. As a consequence of the momentum-dependent pairing, the energy gap will in general be anisotropic on the Fermi surface. In conventional superconductors the pairing potential is usually always attractive and, as a consequence, the gap function is positive and its phase is zero.

A particular anisotropic gap structure, called anisotropic s -wave, is shown (for simplicity in the 2D form) in Figure 1.

Since the electrons involved in the pairing are those in the vicinity of the Fermi surface, the " angular momentum representation" [9] will be used from now on. In this way, different OP

1 Here we still use the acronym " BCS" meaning that the basic assumption of a weak electron-boson coupling is still valid; nevertheless, the addition of a -dependence in the gap is not accounted for by the original BCS paper.

symmetries can be easily expressed through the variable ϕ, so that $\boldsymbol{k}=k_F(\cos\phi,\sin\phi)$. Within this representation, the anisotropic s -wave pairing can be expressed as

$$\Delta(\phi)=\Delta_0\left[(1-\epsilon)+\epsilon\cos(2\phi)^4\right] \tag{3}$$

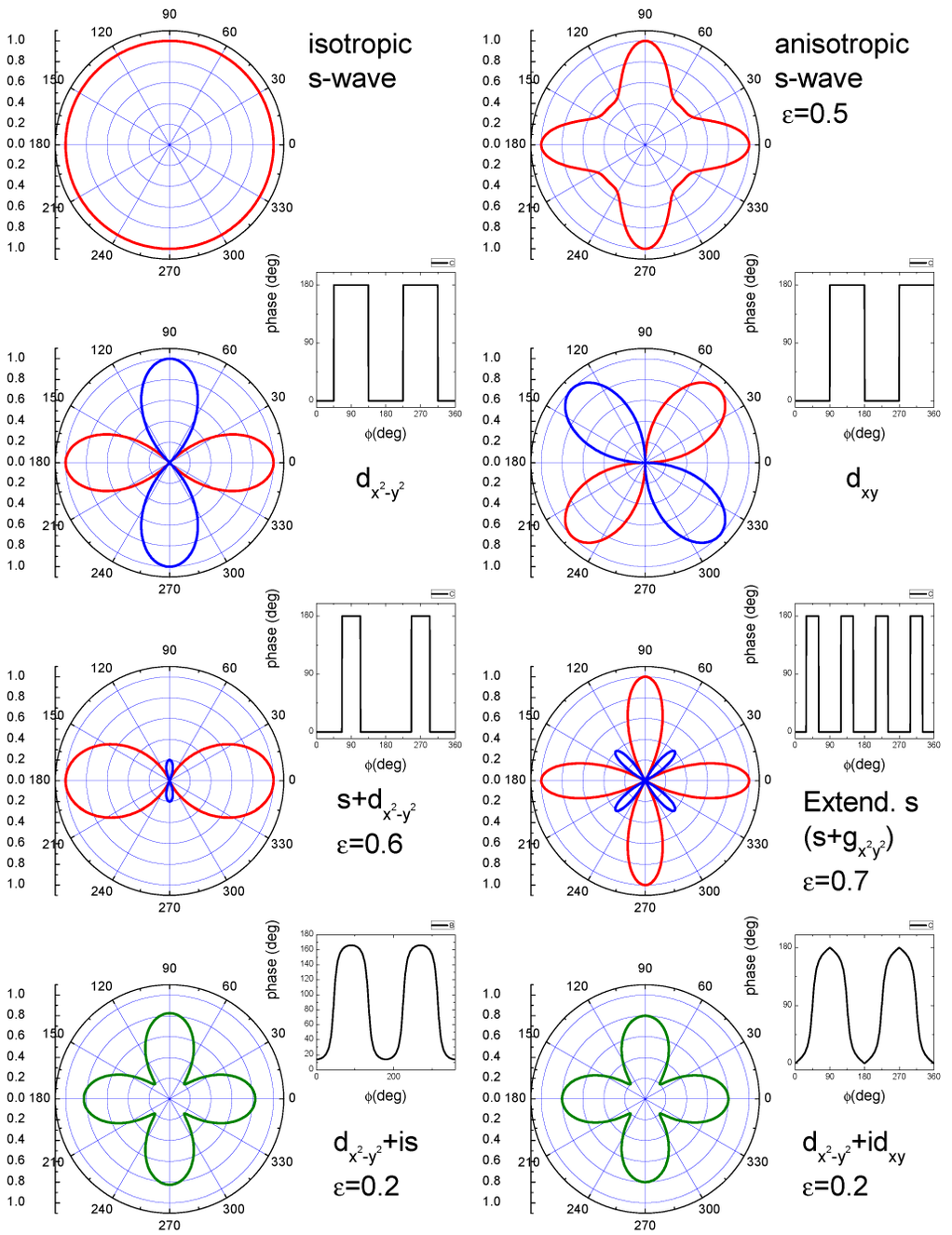

Figure 1. Polar plots of the amplitude of the order parameter for different symmetries and plot of the phase as a function of the angle ϕ. In the case of s -wave symmetry and anisotropic s -wave symmetry the phase is constant and equal to 0 and thus has not been plotted. Red: positive amplitude. Blue: negative amplitude. Green: absolute value of the order parameter for mixed symmetries with imaginary component.

http://dx.doi.org/10.5772/59587

Figure 1 reports the function for =0.5.

After the discovery of the cuprate superconductors more exotic symmetries were investigated in which the gap function can vary in phase and even change sign. The locus of points in the reciprocal space where the gap function changes sign is called nodal line and when nodal lines intersect the Fermi surface the OP is said to be nodal, as it occurs, for example, in some cuprate superconductors (see section 4.1). Another interesting situation can take place when the material features multiple FS sheets that, however, do not intersect the nodal lines. In this case the gaps can feature opposite sign on different FS sheets. As it will be shown in a short while and in section 4.2, this particular gap structure has been theoretically predicted for several Fe-based superconductors (FeBS).

$\Delta(\boldsymbol{k})$ can be expanded in a series of spherical functions, which are often labeled as atomic orbitals (s, p, d, f, $g$etc.). Not every symmetry is allowed in a certain compound. First of all, if the pairs are spin singlets only s -, d -, g -wave symmetries and so on are allowed. Then, depending on the symmetry of the lattice under consideration, only some of them (and their admixture) are possible [10]. The situation in which the symmetry of the order parameter is lower than that of the crystal is usually referred to as unconventional pairing. From now on we will consider only spin-singlet types of pairing as this will be the case for cuprates and FeBS, discussed later on.

The d -wave symmetry can either be of the $d_{x^2-y^2}$ or d_{xy} type. In the first case, the gap function can be written as $\Delta(\phi)=\Delta_0\cos(2\phi)=\Delta_0[\cos(\phi)^2-\sin(\phi)^2]$. The function is real and features line nodes at $\phi=45+n\pi/2$ where it changes sign from positive (red in Figure 1) to negative (blue). On the other hand, the d_{xy} -wave symmetry is expressed in angular coordinates as $\Delta(\phi)=\Delta_0\sin(2\phi 2\Delta_0(\cos\phi\sin\phi)$ and has node lines at $\phi=n\pi/2$. It is easy to see that it corresponds to the previous one but rotated by 45° in the plane, as shown in Figure 1.

Mixed symmetries have also been proposed. For example, an $s+d_{x^2-y^2}$-wave symmetry, where $\Delta(\phi)=\Delta_0[(1-)+\cos(2\phi)]$ or complex admixtures like $d+is$ or $d+id$ have been considered while interpreting PCARS data in cuprates (section 4.1). Some of them are shown in Figure 1.

If the Fermi surface is made up of multiple sheets the gap can be different on each of them and, generally, also be $\boldsymbol{k}$ -dependent on the single sheets. This situation is called multi-band or multi-gap superconductivity which can therefore be regarded as a particular case of anisotropic superconductivity. The BCS weak-coupling formulation was generalized to the multi-band case at the end of the '50s [11, 12]. Assuming the potential to be different on two bands, 1 and 2, but constant on each of them, the disjoint representation can be used and from equation 2 the two gap parameters, in turn constant on each band, can be obtained [13]:

$$\begin{aligned}\Delta_1 &= \Lambda_{11}\Delta_1\int_0^{k_B\theta_D} d\epsilon \frac{\tanh\left(\sqrt{\epsilon^2+\Delta_1^2}\,/2k_BT\right)}{\sqrt{\epsilon^2+\Delta_1^2}} + \Lambda_{12}\Delta_2\int_0^{k_B\theta_D} d\epsilon \frac{\tanh\left(\sqrt{\epsilon^2+\Delta_2^2}\,/2k_BT\right)}{\sqrt{\epsilon^2+\Delta_2^2}} \\ \Delta_2 &= \Lambda_{22}\Delta_2\int_0^{k_B\theta_D} d\epsilon \frac{\tanh\left(\sqrt{\epsilon^2+\Delta_2^2}\,/2k_BT\right)}{\sqrt{\epsilon^2+\Delta_2^2}} + \Lambda_{21}\Delta_1\int_0^{k_B\theta_D} d\epsilon \frac{\tanh\left(\sqrt{\epsilon^2+\Delta_1^2}\,/2k_BT\right)}{\sqrt{\epsilon^2+\Delta_1^2}}\end{aligned} \tag{4}$$

assuming that the cut-off phonon frequency is the same for the two bands. Here, $\Lambda_{ij}=V_{ij}N_j$ where the averaged pairing potential V_{ij} is called intraband if $i=j$ and interband if $i\neq j$.

In order to better understand multi-gap superconductivity and the many different situations that may stem out of equations 4 let us briefly take into consideration two examples of multi-band superconductors, MgB_2 and FeBS. MgB_2 is certainly the clearest example of two-band, two-gap superconductor. It features two (groups of) bands, $\sigma$and π. The σ band would be superconducting on its own, thanks to a considerable electron-phonon intraband pairing, $NV_{\sigma\sigma}$, while the π band would not. However, a small amount of *interband* coupling, $NV_{\sigma\pi}$ couples the σ band to the π one which is made superconduct by the first.

Completely different is one of the most popular scenario invoked to explain superconductivity in FeBS [14]. The intraband electron-phonon coupling is thought to be too small to set superconductivity in [15], but a predominant *repulsive* interband coupling (likely of magnetic origin) can drive the hole-like and electron-like FS sheets into the superconducting state, giving rise to a gap function of opposite sign on the two types of bands. It is worth noticing that this situation occurs in the framework of the s -wave symmetry, but, because of this sign-changing gap, is referred to as$s_{\pm}$. Within this symmetry, the occurrence of " accidental nodes" has been predicted and experimentally observed in particular situations, depending on fine details of the pairing interaction and on the specific electronic structure. Therefore, i) a multi-band model can give rise to extremely diverse situations as far as the OPs are concerned and, in particular, ii) even within the same symmetry, s-wave for instance, the OPs can feature very different *structures* [16]. As we will see for FeBS in 4.2, different gap structures could imply very dissimilar pairing mechanisms of superconductivity.

2.2. The energy-dependent OP in the Eliashberg theory

In 1960 Eliashberg built [17, 18, 19] a strong-coupling generalization of the BCS theory. The Eliashberg theory is still based on the electron-phonon interaction, but relaxes the requirement that this interaction is weak. As a result, the theory accounts for the renormalization of the electron mass arising from the electron-phonon interaction. The Eliashberg theory takes into account the exact electron-phonon spectral function, $\alpha^2F(\boldsymbol{k},\boldsymbol{k}',E)$ and the energy dependence of the gap function, $\Delta(\boldsymbol{k},E)$.

By introducing the Gor'kov F function and working simultaneously with the Green function G and F, Eliashberg could apply the standard perturbation theory to the superconducting state and obtain a 2×2 matrix self-energy correction. The diagonal terms are called $\Sigma(\boldsymbol{k},E)$ and the off-diagonal ones are $\Delta(\boldsymbol{k},E)$. The poles of the Green functions are located at $\pm((E_{\boldsymbol{k}}+\Sigma_{\boldsymbol{k}})^2+\Delta_{\boldsymbol{k}}^2)^1$ and correspond to the single particle excitations (hole-like and electron-like). $\Sigma_{\boldsymbol{k}}$is interpreted as a shift in the generalized BCS excitation energy due to interactions between electrons and $\Delta_{\boldsymbol{k}}$ as the energy-dependent gap function [7]. The complete expression of the Eliashberg equations goes beyond the scope of this chapter but what is important to retain here is that now the order parameter is a complex function of the energy. For example, after averaging over the Fermi surface (in the case of an isotropic OP), we obtain

http://dx.doi.org/10.5772/59587

$$\Delta(E) = Re\left[\Delta\left(E\right)\right] + i\,\mathrm{Im}\left[\Delta\left(E\right)\right] \tag{5}$$

The imaginary part of Δ increases with the increase of the electron-boson coupling and takes into account the finite lifetime of the Cooper pairs. Another interesting quantity is the electron-phonon coupling constant, λ defined, in the isotropic case, as $\int_0^\infty [2\alpha^2 F(E)/E]dE$. λ gives an estimation of the electron-boson coupling and can be related to the original BCS pairing parameter by $NV \equiv (\lambda - \mu^* 1 + \lambda)$, where μ^* is a purely electronic quantity referring to the average Coulomb potential on the Fermi surface. As it will be shown later, in case of strong-coupling superconductors, the energy-dependence of the order parameter can manifest itself in the tunneling or point-contact spectra, possibly giving important hints about the pairing mechanism.

It is also possible to account for the gap anisotropy within the Eliashberg theory even though this can be very demanding from the computational point of view [20]. In this regard, it is worth recalling a method developed by P.B. Allen, that adopts a particular set of functions, called Fermi-surface harmonics, that can considerably simplify the solution of the Eliashberg equations in this case [21, 22].

3. Point-Contact Andreev Reflection Spectroscopy (PCARS)

Point-contact spectroscopy (PCS) was developed in the '70s [23], especially for studying the electron-phonon interaction in metals. It was found out later though, that it could be used to study many kinds of quasi-particle excitation and scattering mechanism, like the electron-magnon interaction, crystal-field excitations, scattering with magnetic impurities and so on [24]. Then, especially after the theoretical work of Blonder, Tinkham and Klapwijk in 1982 [25], it also turned out to be a very powerful and unique method for studying the order parameter in superconducting materials.

There already exist some very comprehensive reviews or books on point-contact spectroscopy in the literature where very detailed and exhaustive information about the technique and its achievements can be found [24, 26 - 29]. The reader who wants to study PCS in greater detail can refer to those. Below we will only report some basic information that will help to better follow the issues addressed in section 4.

3.1. Point-contact spectroscopy: Ballistic, thermal and diffusive regime

There are several different ways of fabricating point contacts [24] but one of the most popular is the so-called needle-anvil or " hard" PCS technique. It consists of gently pressing a very sharp metallic tip against the material under study so as to create a " small" (point-like) contact, and in measuring the $I-V$ characteristics across the junction thus formed. However, it is also worth mentioning here another technique, called " soft" PCS technique [30]. The soft PCS consists in making the point contact by using a small drop of silver paint put on the sample surface instead of the metallic tip. This method can be used even on brittle samples or very

thin films because no pressure is applied (hence the name " soft"). Moreover, it ensures a higher thermal and mechanical stability and, by applying short voltage or current pulses (fritting), the properties of the contact can often be tuned.

The principle of PCS (in normal metals) is that the quasi-particle that enters the material under study through the contact can be scattered by elementary excitations. This process leaves its fingerprints in the $I-V$ characteristics of the contact, that allow determining the energy spectrum of the excitations. Of course, for the whole process to be meaningful, the energy of the injected quasi-particles must be well known and this is true only if they do not lose energy through scattering in the contact region. In this regard, the situation when they don't scatter inside the contact region is called *ballistic regime* and is the ideal condition for getting good spectroscopic data. The *diffusive regime* occurs when they instead undergo elastic scattering in the contact. In this case it is still possible to observe energy-resolved quasi-particle scattering but the signal will likely be lower. Finally, when electrons scatter inelastically inside the contact region information regarding their energy is lost, the contact can get considerably heated and spectroscopy is definitely hampered: it is the *thermal regime*. If we model the contact area by a circular orifice of radius a, the ballistic regime is defined by the condition $a \ll \ell_e$, the diffusive by $a \ll \Lambda$ and the thermal one by $a \gg \ell_i$. ℓ_e and ℓ_i are the elastic and inelastic electronic mean free paths, respectively and Λ is the diffusion length, $\Lambda=\sqrt{\ell_i \ell_e}$.

In the ballistic regime the resistance of the contact can be described by the Sharvin resistance $4\rho\ell 3\pi a^2$), where ρ is the resistivity and, in case of contacts between different materials (heterocontacts), the product $\rho\ell$ is that of the bank with the smaller Fermi energy [26]. From this formula it is possible to determine if a contact fulfills the ballistic condition, $a \ll \ell$, by comparing the experimental resistance across the contact R_N with the condition $R_N \ll 4\rho 3\pi\ell$). It is worth noticing though, that if the contact does not fulfill the above condition, it does not necessarily mean that the regime is not ballistic. Indeed, the actual contact can likely be the parallel of several nano-contacts so that the condition here reported can be regarded as an upper limit. When it is not fulfilled, one has to look at other experimental features that could allow to conclude that the contact is ballistic. For instance, heating effects should be absent. In particular, if the differential resistance of the contact as a function of the voltage drop across the contact has the same functional form of the resistivity as a function of the temperature, then the contact is most probably in the thermal regime.

When point contact measurements are carried out in the superconducting state, the process that allows determining the energy of the superconducting gap is either Andreev reflection or quasi-particle tunneling, depending on the height of the potential barrier at the interface. In any case, the spectroscopic information is energy-resolved only if the contact (in the normal state) is in the ballistic or at most diffusive regime. In the Andreev reflection regime, another condition is generally to be fulfilled, i.e. $a \ll \xi$, where ξ is the superconducting coherence length. This is necessary to avoid that superconductivity in the vicinity of the contact is destroyed by the injected current, which in that region may become overcritical [28].

3.2. PCS in superconductors: The BTK model and beyond

Point-contact spectroscopy can be a very powerful technique to probe the order parameter in superconductors mainly thanks to the existence of the Andreev reflection [31], a quantum

http://dx.doi.org/10.5772/59587

process that occurs at the interface between a normal metal N and a superconductor S. To explain the Andreev reflection in a nutshell, let us consider an electron incoming from N with an energy $eV < \Delta$. When it reaches the $N-S$ interface (that we now suppose perfectly ideal, i.e. with no potential barrier) it cannot be transmitted into S as a quasi-particle, as there are no allowed energy states in that energy range. It is then reflected as a hole (Andreev reflection) and, to conserve the charge balance, a Cooper pair is transmitted in S. This fact is equivalent to a doubling of the conductance at voltages $V < \Delta / e$. If the energy of the incoming electron is instead $eV > \Delta$ it can be transmitted as a quasi-particle and the conductance is that of an $N-N$ junction. It is clear then that the " change of slope" in the conductance occurs at energies corresponding to the energy gap whose amplitude can thus be estimated.

In 1982, Blonder, Tinkham and Klapwijk (BTK) gave the first satisfactory theoretical description of the Andreev reflection occurring in $N-S$ microconstrictions [25] that can be compared to experimental point-contact data. By solving the Bogoliubov-de Gennes (BdG) equations, BTK were able to calculate the probability coefficients of the transmission and reflection of the quasi-particles at the $N-S$ interface. In particular, the Andreev reflection is one of the processes that come out from the solution of the BdG equations. Noticeably, they also took into account the effect of a potential barrier at the interface, so that the complete transition from the ideal Andreev reflection (metallic contact, with no barrier) to the tunneling regime (thick barrier) was modeled. Also, two more processes can occur at the interface in the presence of a barrier which are called normal and " anomalous" reflection. In the BTK model, the potential barrier is taken into account by a dimensionless parameter $Z = U_0 / (\hbar v_F)$, where U_0 is the height of the potential barrier, represented by the repulsive potential $U_0 \delta(x)$ localized at the interface [25]. Note that although Z can be defined in this (rather abstract) way, BTK themselves underline that it should rather be thought of as a phenomenological parameter when comparing the predictions of their model to experimental data. Z can thus account for any source of elastic scattering in the neck, irrespective of its microscopic origin [32]. Besides considering both the N and S Fermi surface to be spherical, and the gap to have an isotropic s-wave symmetry, the model also assumes the momentum of incoming electrons to be perpendicular to the interface. We will thus refer to this result as the 1D BTK model. The effect of the temperature can be accounted for by a proper convolution of the conductance with the Fermi distribution function [26]. The mismatch of the Fermi velocities between the two sides of the contact can be included in the model by substituting the parameter Z with an effective barrier parameter, $Z_{eff} = \sqrt{Z^2 + [(1-r)^2 4r}$, where $r = v_{F1} / v_{F2}$ is the ratio of the Fermi velocities in the superconducting and in the normal side [32]. Despite its simplicity, the 1D BTK model allowed comparison to experimental data with a fairly good agreement.

Since the BTK model predicted conductance curves with sharper structures and less spread in energy than the actual experiments, a further parameter, Γ, was introduced to represent the reduced quasi-particles lifetime mainly due to i) the presence of an imaginary part in the self-energy (see 2.2 and ref. [33]) and ii) any kind of inelastic scattering at the interface caused by non-ideal conditions (dead layers etc.) [34]. Γ, called the broadening parameter, can easily be introduced into the model by the simple substitution $E \rightarrow E + i\Gamma$.

The unidirectional electron incidence assumed in the 1D BTK model is an oversimplification whenever the system is not perfectly isotropic. In these cases, one has to account for the fact that electrons can approach the interface along any direction. However, if we restrict for the

time being to a plane perpendicular to the interface and call θ_N the angle between the incident electron and the normal to the interface, $\boldsymbol{n}$, the expression for the normalized conductance at $T=0$ is

$$G_{2D}(E)=\frac{\int_{-\frac{\pi}{2}}^{+\frac{\pi}{2}}\sigma(E,\theta_N)\cos\theta_N d\theta_N}{\int_{-\frac{\pi}{2}}^{+\frac{\pi}{2}}\tau_N(\theta_N)\cos\theta_N d\theta_N} \tag{6}$$

where $\sigma(E,\theta_N)$ is the BTK conductance expressed by

$$\sigma\left(E,\theta_N\right)=\tau_N\cdot\frac{1+\tau_N\left|\gamma_+(E)\right|^2+\left(\tau_N-1\right)\left|\gamma_+\left(E\right)\gamma_-\left(E\right)\right|^2}{\left|1+\left(\tau_N-1\right)\gamma_+\left(E\right)\gamma_-\left(E\right)\exp\left(i\varphi_d\right)\right|^2}. \tag{7}$$

$\tau_N(\theta_N)$ is the barrier transparency, defined as

$$\tau_N\left(\theta_N\right)=\frac{\cos\left(\theta_N\right)^2}{\cos\left(\theta_N\right)^2+Z^2}. \tag{8}$$

and

$$\gamma_\pm\left(E\right)=\frac{E-\sqrt{E^2-\left|\Delta_\pm\right|^2}}{\left|\Delta_\pm\right|} \tag{9}$$

Moreover, $\varphi_d=(\varphi_--\varphi_+)$and $\varphi_\pm$ are the phases of $\Delta_\pm$, which in turn represent the pairing potential experienced by electron-like and hole-like quasi-particles (ELQs and HLQs) [35]. The formulation of the BTK conductance reported here [35], which is different from that of the original BTK paper and that we will call 2D BTK model, assumes also that the effective masses in N and S are equal. This formulation is apt to describe Andreev reflection in superconductors with all the symmetries of the OP that can be expressed in polar coordinates in the reciprocal plane (k_x,k_y). For example, the anisotropic s -wave OP would be expressed as

$$\Delta_\pm=\Delta_{is}+\Delta_{an}\cos^4\left[2\left(\pm\theta_N-\alpha\right)\right] \tag{10}$$

and the $d_{x^2-y^2}$ -wave one as

$$\Delta_\pm=\Delta_0\cos\left[2\left(\pm\theta_N-\alpha\right)\right] \tag{11}$$

α being the angle between the normal to the interface and the crystallographic axis a, that we assume to be zero in the configurations shown in Figure 1.

http://dx.doi.org/10.5772/59587

Figure 2a shows the temperature dependence of the 2D BTK conductance for an isotropic s -wave gap while panels c and d report the case for a $d_{x^2-y^2}$ -wave gap with incident angle $\alpha=\pi/4$ and $\alpha=\pi/8$, respectively.

It is important to notice here that when tunneling (in the ab -plane) along the nodal direction in case of nodal symmetries (like $\pi/4$ for a $d_{x^2-y^2}$ -wave OP), the shape of the spectra is very different from the s -wave case reported in panel a. The conductance curves feature a zero-bias conductance peak (ZBCP) that can be, at high Z values, higher than 2 (not allowed for the s -wave case) and that decreases when moving away from the nodal direction. At $\pi/8$ (panel d) it is lower, while other structures appear at finite energy. At the antinodal direction ($\alpha=0$, not shown) the spectra are more similar, when Z>0, to those for an s -wave OP but with a slightly V-shaped dip at zero bias [26].

The ZBCP can be a very important signature of the presence of nodes in the OP and is caused by the formation of zero-energy Andreev bound states (ABS) at the interface, due to the fact that along the nodal direction HLQs and ELQs experience pair potentials $\Delta_{\pm}$ with a phase difference equal to π [35] (see eq. 11).

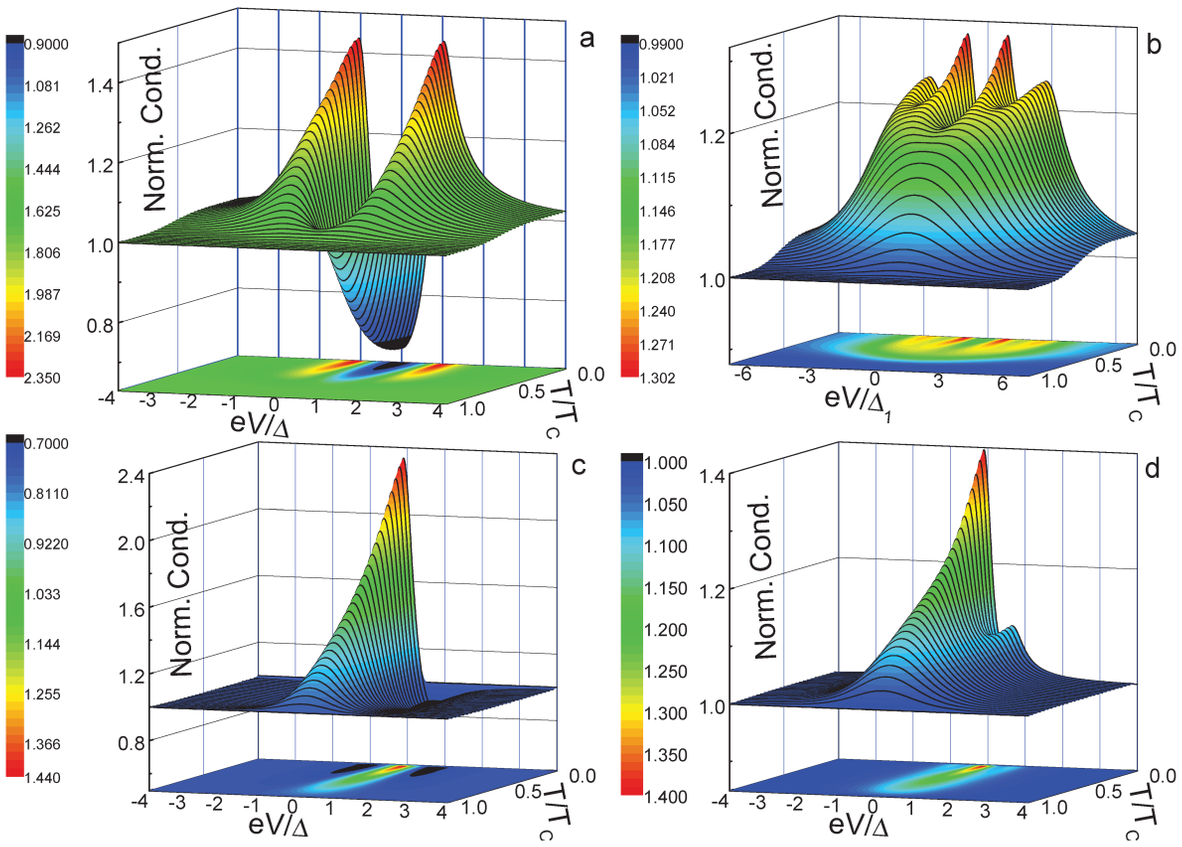

Figure 2. Temperature dependence of the normalized conductance curves calculated within the 2D BTK model for different symmetries of the order parameter. The parameters of the model have been chosen to mimic realistic experimental conditions. (a): isotropic s -wave gap, $\Gamma=\Delta/5, Z=0.8$. (b): two isotropic s -wave gaps with the sameT_c, $\Delta_2=3\Delta_1$, $\Gamma_i=\Delta_i/5$, $Z_i=0.4$, $w_1=0.5$. (c) $d_{x^2-y^2}$-wave gap, $\Gamma=\Delta/5$, $Z=1.2$, $\alpha=\pi/4$. (d): same as in c but now $Z=1.0$ and $\alpha=\pi/8$.

In some cases (for example when Z is low, or broadening effects are taking place) the ZBCP can be smeared out and look like a maximum rather than a peak. In these conditions, the Andreev spectra for the d -wave symmetry become very similar to those expected, for example, in the case of anisotropic s -wave gap with zeroes on the Fermi surface [27]. Moreover, as we will better see below, symmetries like the d -wave and the fully anisotropic s -wave can also appear similar when injecting the current along the c axis.

There may also be situations when, even though the OP features nodal lines, ABS don't occur because the line is, for instance, away from the Γ point in the first Brillouin zone and HLQs and ELQs always see the same sign of the OP. This is the case, for example, of $CaFe_2A_2$ under pressure [36], discussed in section 4.2.

Finally, panel b of Figure 2 shows the temperature dependence of the conductance calculated within a two-band, 2D BTK model with two isotropic s -wave gaps with the same T_c. In this case the total conductance is simply the weighed sum of the contribution of the two bands, $G_{Tot}=w_1G_1+(1-w_1)G_2$, where w_1 is the weight of band 1 and $G_{1,2}$ are expressed by eq. (6).

The 2D BTK model has been commonly used to fit the PCARS spectra of various unconventional superconductors, namely cuprates, with a d -wave or a mixed symmetry of the OP. Cuprates being essentially 2D materials, with a cylindrical Fermi surface, this approach is justified. In other materials, however, like FeBS, the assumption of spherical or cylindrical FS is untenable and the 2D BTK approach, even if generalized to the multiband case, is necessarily approximated. It is actually possible to take into account arbitrary incident directions by adding an integration over the inclination angle ϕ. Following refs [37, 38], the most general formula for the conductance in the 3D case at $T=0$ can be expressed as [26]:

$$\left\langle G(E)\right\rangle_{I\mathbf{Pn}}=\frac{\sum_i\left\langle\sigma_{i\mathbf{k}n}(E)\tau_{i\mathbf{k},n}\frac{v_{i\mathbf{k},n}}{v_{i\mathbf{k}}}\right\rangle_{FS_i}}{\sum_i\left\langle\tau_{i\mathbf{k},n}\frac{v_{i\mathbf{k},n}}{v_{i\mathbf{k}}}\right\rangle_{FS_i}} \tag{12}$$

where

$$\tau_{i\mathbf{k},n}=\frac{4v_{i\mathbf{k},n}v_{N,n}}{\left(v_{i\mathbf{k},n}+v_{N,n}\right)^2+4Z^2v_N^2} \tag{13}$$

Here i indicates different FS sheets and the brackets an average over the i -th sheet. $\boldsymbol{n}$is the direction of current injection, $v_{i\boldsymbol{k},n}=\boldsymbol{v}_{i\boldsymbol{k}}\cdot\boldsymbol{n}$ is the projection, along $\boldsymbol{n}$, of the velocity on the i -th sheet. In the formula for $\tau_{i\boldsymbol{k},n}$, which is the normal-state barrier transparency, $v_{N,n}=\boldsymbol{v}_N\cdot\boldsymbol{n}$, $\boldsymbol{v}_N$ is the Fermi velocity of the normal material, assumed constant. $\sigma_{i\boldsymbol{k}n}(E)$is similar to eq. (7) but now τ_N is expressed as in eq. (13) and $\Delta=\Delta_{i\boldsymbol{k}}$. The calculation of the conductance in this case can be very demanding from the computational point of view and, in principle, requires the knowledge of the k -dependence of the order parameter on the whole FS. Therefore, we developed a method [27, 29] that under some assumptions and simplifications allows writing eq. (12) and (13) in the form of integrals over the angles θ and ϕ provided that: i) the different

http://dx.doi.org/10.5772/59587

FS are modeled by means of suitable 3D surfaces like hyperboloids, ellipsoids and so on, and ii) $\Delta(k)$admits a simple analytical expression in the same coordinates. It is in this way possible to perform the fitting procedure in an easier way. This model, in some cases, allows obtaining interesting information regarding the actual shape of the FS and the OP symmetry. For example, when the current is injected along the c -axis in superconductors with warped cylindrical FS sheets the conductance doesn't show ZBCPs for a d -wave OP because ELQs and HLQs feel the same sign of the OP. But neither the zero-bias maximum (that would be expected since the gap is zero in some regions of the FS) is observed. Instead, a zero-bias *minimum* occurs [27]. The same happens for OPs with full in-plane anisotropy, so that these two symmetries are almost impossible to distinguish by c -axis PCARS measurements. Only in-plane measurements can help discriminating between a d -wave and a fully-anisotropic s -wave, since only in the former ZBCPs due to Andreev bound states are expected at nodal directions.

Seen the other way around, if a superconductor has at least one FS sheet with line nodes in the OP and the conductance curves along the c axis feature zero-bias maxima, it means that the relevant FS sheet has a 3D character [27, 36]. As it will be shown in section 4.2, this is the case of $CaFe_2As_2$ under pressure and Co-doped $CaFe_2As_2$.

When tunneling along the c axis in cuprates, the situation is slightly different. Here, because of the perfectly 2D nature of the Fermi surface, the final states have only transverse wavevector [39] so that the conductance must be calculated by integration over the entire (k_x,k_y) plane. No ZBCP is thus expected to occur, and again – if some broadening is present or the barrier parameter is low – the d -wave symmetry might not be distinguishable from a symmetry with zeroes. Also in this case, measurements in the ab plane could be necessary to detect the possible presence of ABS and thus of gap nodes.

We have seen in section 2.2 that the actual order parameter is energy-dependent and that when the electron-boson coupling is strong enough the PCARS conductance can feature typical structures that arise from the spectrum of the bosonic excitations that may serve as a pairing glue. Indeed these features appear at the relevant boson energy, $\Omega_b$in the density of states that can be directly measured in tunneling experiments. Since the BTK model can also describe tunneling experiments when the barrier is large enough, it is possible to introduce the energy-dependent expression of the OP in equation 9. The electron-boson interaction (EBI) features in the conductance persist with decreasing values of Z (Andreev reflection regime) and appear at energies of about $\Delta + \Omega_b$ in single-band superconductors [26], while the situation can be more complex in multi-band ones [27]. However, as it will be shown in section 4.2.1, they can be nevertheless interpreted and convey important information regarding the pairing mechanism also in case of (strong-coupling) multi-band superconductors.

4. PCARS in High-Tc superconductors

4.1. PCARS in Cuprates

In cuprate superconductors, point contact spectroscopy has been used to address various fundamental issues concerning the superconducting order parameter, i.e. its amplitude, its

symmetry (and its possible change as a function of doping) and its relationship with the pseudogap (PG). As far as the latter point is concerned, the sensitivity of Andreev reflection to the phase coherence has provided complementary information to tunneling and STM experiments that probe instead the unpaired quasi-particles. As a result, the (superconducting) gap probed by PCARS and that closes at T_c differs significantly from the (pseudo)gap measured by tunnel spectroscopy at low temperature, and that can persist well above T_c (in hole-doped cuprates). While the former scales with the critical temperature (thus showing a maximum at optimal doping, OPT) the second decreases monotonically with increasing doping until they merge or become comparable at a critical doping (that in most cases is slightly above the optimal one), as shown in Fig. 3 f. Actually, the gap vs. pseudogap issue is very complicated, especially as for whether the pseudogap is associated to pre-formed pairs with no phase coherence (that however determine a suppression in the quasi-particle density of states around the Fermi level) or is instead unrelated to superconductivity. For a discussion of this issue please see [40, 28] and references therein.

As noticed in ref. [28], the observation of Andreev reflection itself in cuprates leads to some interesting conclusions: i) the Bogoliubov-de Gennes equations hold for these materials, and thus a fermionic description is appropriate for them; ii) the large mismatch in Fermi velocities between the normal counterelectrode and the cuprates, that should suppress Andreev reflection [41], in reality does not, because the renormalization of the Fermi velocity in the point-contact experiments differs from the full quasi-particle normalization (by the way, the same happens in heavy fermion superconductors); iii) Andreev reflection occurs in cuprates even though they do not fulfill the BCS condition $\Delta \ll E_F$ (especially in the underdoped, UD, regime) and are rather close to a transition to a Bose-Einstein condensation. It is clearly impossible here to account for all the published results; for further more detailed information, we suggest the very good reviews by Deutscher (mainly focused on hole-doped cuprates [40, 28] and Armitage *et al.* [42](focused on electron-doped cuprates).

As for the symmetry of the OP, it seems now well established that hole-doped cuprates have a superconducting OP with dominant $d_{x^2-y^2}$ symmetry (with nodes along the (110) direction) and, sometimes, minor imaginary contributions like is of id_{xy} that break the time-reversal symmetry [10]. There has been a long debate about the intrinsic (bulk) or extrinsic (related to the surface) origin of this additional component, and about the doping range in which it exists, as will be briefly mentioned in the following.

In $YBa_2Cu_3O_{7-}$ (YBCO), one of the most studied cuprates, early directional PCARS measurements in single crystals gave evidence of a ZBCP along the nodal direction (110) and of two Andreev maxima along the antinodal direction (100) [39], results confirmed by STM measurements in the same configurations (see fig.3a). The PCARS spectra were successfully fitted with the 2D BTK model by Tanaka and Kashiwaya for the case of a pure d -wave symmetry, which gave an energy gap of amplitude $\Delta \simeq 28$ meV and also set an upper limit of 5% for the weight of any possible isotropic OP component (s or is). In general, PCARS measurements away from the nodal direction are in very good agreement with a pure d -wave symmetry. However, later PCARS measurements along (100) in $Y_{1-x}Ca_xBa_2Cu_3O_{7-}$ crystals were shown to require (even for $x=0$) a $d+is$ fit [43] in which the relative amplitude of the s (d) component increased (decreased) with decreasing the barrier parameter Z (see fig.3b and c) independent

http://dx.doi.org/10.5772/59587

of the critical temperature or of the Ca content of the sample. In other words, an almost pure d -wave symmetry was found approaching the tunneling regime, while a substantial isotropic component was found in high-transparency contacts. This puzzling result was explained in terms of an unusual proximity effect that induces an s -wave OP in the normal metal, and on the S side depresses the d -wave component and enhances the (presumably preexisting) subdominant is -wave OP component [43, 28]. The emergence of the subdominant is component in the OP at the surface of YBCO was indeed predicted theoretically [44], unrelated to proximity effects and thus intrinsic to this material. Its most striking effect is to break the time-reversal symmetry, leading to spontaneous supercurrents that flow on the surface of the crystal, and that result in a Doppler shift of the Andreev bound states to finite energy. Thus, the ZBCP (that would be seen along the nodal direction for a pure d symmetry) spontaneously splits. This splitting has indeed been observed in some measurements [45] (see fig. 3d), but not in others [46]. In various cases a splitting was seen only in the presence of magnetic fields (and, moreover, in conditions where the surface screening supercurrents were presumably negligible, which would indicate that the subdominant imaginary component in the OP is not due to the Doppler shift of the ABS but is induced by the field itself) [47, 28]. STM measurements in Ca-YBCO films with (110) orientation at different doping levels finally showed that the spontaneous splitting occurs only in the overdoped (OD) regime, suggesting a doping-induced transition from pure d wave to a mixed $d + is$ or $d + id$ symmetry (with the imaginary component being no more than 10% of the main real component) [46]). Incidentally, this points towards a bulk nature of the subdominant component; its emergence could be due to an actual change in the pairing interaction within a quantum critical point scenario [28].

In $La_{2-x}Sr_xCuO_4$ (LSCO) the anisotropy of the OP is suggested by several experimental techniques such as specific heat, ARPES, Raman scattering, magnetoresistance. Strictly speaking, however, these do not prove that the gap has nodes. On the other hand, evidence *against* gap nodes in LSCO near optimal doping ($x = 0.15$) was given by early tunneling measurements in single-crystal break junctions. PCARS measurements in LSCO single crystals near optimal doping along the (110) direction did not show the expected ZBCP but rather two symmetric conductance maxima at 3-5 meV and a general shape that is incompatible with both the pure s -wave and the pure d -wave symmetry [48], and excludes any symmetry with nodes. A good fit of the spectra was obtained with an $s + d$ symmetry or an *extended* s -wave (with no zeros). A similar conclusion was later drawn for the *whole* doping range, from underdoped to overdoped – even though some PCARS measurements in underdoped crystals provided evidence of a ZBCP disappearing at a temperature T_c^* much lower than the bulk T_c, and which was well fitted to a pure d -wave symmetry of amplitude $\Delta = 5\,\text{meV}$ assuming $I \parallel (110)$ [28]. Stimulated by these results, we performed PCARS measurements in polycrystalline samples of LSCO with six different compositions, from underdoped to overdoped, by using a sharp Au tip pressed against the sample. The spectra gave no evidence of ZBCP and instead suggested, again, the absence of nodes in the whole superconducting dome. As a matter of fact, the shape of 100% of the spectra is absolutely incompatible with a pure d -wave symmetry (see fig.3e); they all show symmetric conductance maxima and some of them are very similar to those obtained in [48]. It is clear, even from the position of the maxima, that the gap amplitude has a maximum at optimal doping. The curves are best fitted by using either a $s + d$ symmetry [49] with a dominant *isotropic* component, or a $d + id$ symmetry [50] (even though a

pure s -wave fit is not too bad at least in some cases). In the latter case (preferable, since the compatibility of $s+d$ symmetry with the low-temperature lattice structure of LSCO is questionable) the d_{xy} component follows the trend of T_c as a function of Sr concentration and has thus a maximum at optimal doping, while the $d_{x^2-y^2}$ component tends to saturate to a constant value on increasing x [50] as shown in fig.3f. A strong suppression of both the $d_{x^2-y^2}$ component and of the gap magnitude $|\Delta|$ occurs at $x1$, where also T_c is reduced, further indicating a close relationship between the Andreev gap and the critical temperature.

The $d_{x^2-y^2}+id_{xy}$ symmetry that allows fitting our data is thus the same proposed for YBCO above optimal doping, and also invoked to explain the field-induced splitting of the ZBCP in YBCO and BSCCO. The conditions leading to the quantum phase transition from a pure $d_{x^2-y^2}$ to a mixed $d_{x^2-y^2}+id_{xy}$ one (with a smaller d_{xy} component) were indeed find to occur in LSCO in a small doping range from $x=0.19$ up to $x=0.24$, thus slightly shifted in the overdoped regime. Our results seem instead to indicate that the mixed symmetry is robust against doping, and persists in the whole superconducting dome (which also contrasts with the findings in YBCO). Since our junctions are all in the low- Z regime, an anomalous proximity effect (already discussed above for YBCO) cannot be excluded as the origin of the subdominant imaginary OP component [43]. This could be the case since more recent PCS measurements in underdoped LSCO in the tunneling (high Z) regime [51] have given spectra with symmetric conductance maxima in the (100) direction and a clear ZBCP in the (110) direction, as expected for a pure d -wave symmetry. It is worth noting that, in any case, these findings confirm that the gap measured by PCARS is different from that measured by tunnel or ARPES measurements, which decreases monotonically with doping (see fig.3f and g).

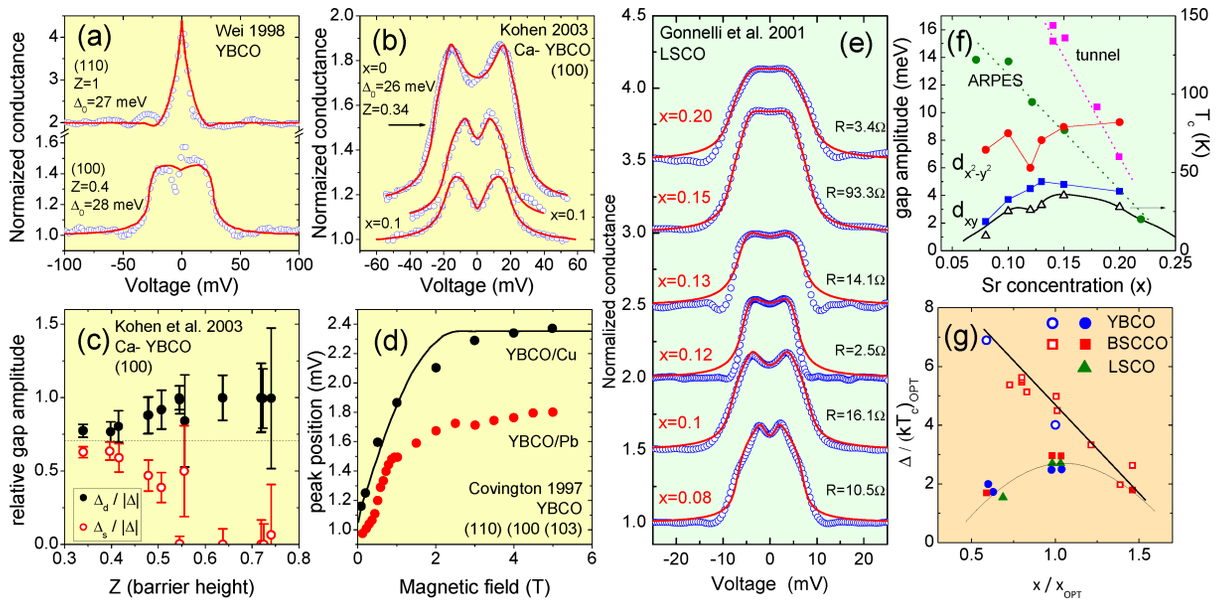

Figure 3. (a) Examples of PCARS spectra in YBCO along the nodal (110) and the antinodal (100) direction, with the relevant fit to a 2D BTK model with a pure d -wave symmetry (from [39]). (b) PCARS spectra in $Y_{1-x}Ca_xBa_2Cu_3O_{7-}$ crystals along the (100) direction with the relevant fit to a $d+is$ symmetry (from [43]). (c) Amplitude of the s and of the d -wave components as a function of the barrier parameter Z (from [43]), suggesting that the subdominant imaginary

http://dx.doi.org/10.5772/59587

component may be originated by an anomalous proximity effect. (d) Position of the peak observed in (110) tunneling spectra in YBCO as a function of the magnetic field. Notice that even in zero field the peak does not occur at zero bias (from [45]). (e) PCARS spectra in LSCO at various doping levels, and the relevant fit with a $d_{x^2+y^2} + id_{xy}$ symmetry (from [49, 50]). (f) Doping dependence of the $d_{x^2+y^2}$ and d_{xy} gap amplitudes compared to that of T_c and of the gap measured by tunnel and ARPES (from [49, 50]). (g) Normalized amplitude of the phase-coherence gap from Andreev reflection (solid symbols) and of the single-particle excitation gap (open symbols) for different cuprates (from [48, 28]).

Electron-doped cuprates (in which carriers are predominantly electrons) have general formula $R_{2-x}M_xCuO_4$ where R is a rare earth (Pr, Nd, Sm, Eu) and M is Ce or Th. The most studied are $Nd_{2-x}Ce_xCuO_4$ (NCCO) and $Pr_{2-x}Ce_xCuO_4$ (PCCO). These materials differ from hole-doped cuprates in many respects, among which: i) the lattice structure; ii) the maximum critical temperature (much lower in n-doped ones); iii) the phase diagram (e.g. the antiferromagnetic phase typical of the parent compounds persists upon much higher doping and even crosses the superconducting dome). Because of these and other differences, a straightforward generalization of the results obtained on hole-doped cuprates to the electron-doped cuprates is not reasonable. A careful investigation of the OP symmetry became possible only with the synthesis of high-quality samples. The most direct and convincing evidence of d -wave symmetry in PCCO came from tricrystal grain-boundary junction and ARPES measurements, but conflicting results indicating an s -wave symmetry were collected as well, for example by penetration depth measurements. In-plane PCARS measurements were carried out in c -axis oriented films of PCCO at different doping by Biswas *et al.* [52]. The precise direction of current injection in the *ab* plane was unknown. In the whole doping range, from UD to OD, high- Z contacts gave tunnel-like spectra with a zero-bias conductance minimum, coherence peaks at finite energy, and no ZBCP. Low- Z spectra were instead doping-dependent. In UD films they showed a single ZBCP (whose width was of the order of the gap amplitude) that was suppressed, but did not split, in a magnetic field parallel to (001). In OPT and OD samples, they displayed Andreev-reflection features in the form of symmetric maxima typically associated to a nodeless gap. This behavior was interpreted as suggesting a doping-induced transition between $d_{x^2-y^2}$ and s -wave (or a nodeless $d + is$) symmetry, despite a number of unexplained anomalies. Shan *et al.* carried out PCS measurements (with a metallic tip) in the tunneling regime in NCCO single crystals at optimal doping [51]. They unexpectedly obtained very similar spectra along the (110) and the (100) direction, characterized by: i) clear coherence peaks at the gap edges; ii) a shape typical of SIN junctions, with no Andreev-reflection conductance enhancement even at low contact resistance; iii) no zero-bias conductance peak. The spectra along (110) are thus absolutely incompatible with a pure d -wave symmetry that would give a ZBCP and no (or suppressed) coherence peaks. Instead, all the spectra admit an s -wave fit. The resulting gap amplitude turns out to follow the BCS weak-coupling predictions both for its amplitude and its temperature dependence. These results would prove that the OP of NCCO is certainly not pure d -wave; on the other hand, it is very unlikely that it is pure s -wave. Indeed, the fit itself works also with an anisotropic s symmetry or, for instance, by assuming a two-band picture (suggested by ARPES measurements) where one band (crossing the Fermi level at $\pi/2$, $\pi/2$) has an OP with pure d -wave symmetry and the other (at $(\pm\pi,0)$ and $(0,\pm\pi)$) an OP with a s -wave symmetry [51]. Tunneling spectra in SIS c -axis junctions in PCCO carried out by Dagan *et al.* [53] were later shown to be compatible with a non-monotonic d -

wave symmetry (with gap maxima displaced away from the (100) direction, as suggested by Raman spectroscopy and ARPES experiments) in the whole doping range. This symmetry is consistent with the observation of phase-sensitive experiments, even though, exactly as the pure d -wave, it would give a ZBCP due to the presence of ABS along the nodal direction and a marked in-plane anisotropy of the spectra. The lack of both these features in the tunneling experiments was then ascribed to the materials being in the dirty limit ($\xi > \ell$). Interestingly, the gap determined by the fit follows a BCS-like temperature dependence and scales with T_c, with a BCS gap ratio $2\Delta / k_B T_c \simeq 3.5$, thus similar to the one predicted by the BCS theory. According to the authors, this would indicate that PCCO and NCCO are characterized by a weak electron-boson coupling.

4.2. PCARS in Fe-based superconductors

PCARS experiments started being performed on FeBS [54] soon after their discovery and, initially, they were carried out on polycrystalline samples. Indeed the advantage of PCARS with respect to other spectroscopic techniques (namely ARPES and STM) is that it does not require an atomically flat surface. However, early measurements were often contradictory and some authors reported different results regarding the number and symmetry of the OP(s), i.e. single-gap, multi-gap, nodal or nodeless superconductivity. After a while though, also thanks to the availability of higher-quality samples, the multi-band nature of the FeBS became clear even if, in a few cases, it may be difficult to single out more than one gap in the PCARS spectra. Moreover, most of the results seem now in favor of an s -wave type of symmetry that could either feature an s_{++} or $s_{\pm}$ gap structure (characterized by isotropic OPs with different sign on the hole-like and electron-like FS), with possible zeroes or nodes occurring in particular situations.

As for the pairing, since a phonon-mediated mechanism seems to have been ruled out soon [15], the two main possible scenarios are at present a magnetic one (either with itinerant or localized electrons) or a charge/orbital one [66]. In the first case the OP is expected to change sign on different FS sheets, i.e. to have an $s\pm$ structure (even though in some cases it may preserve the same sign on different bands [67]) while in the second the main candidate is the s_{++} wave, with no sign change. Despite great progress has been achieved in a considerably short time, the symmetry and, in particular, the structure of the OP in these compounds appear still rather elusive, maybe even more than it seemed a few years ago. This statement certainly regards PCARS as well, which has been mainly applied up to now to the investigation of the compounds that belong to the 1111 and 122 family, mostly to the latter.

PCARS on 1111 FeBS has been performed mainly on polycrystalline samples or thin films (Figure 4a-c and i) as it is still rather difficult to grow large crystals. To the best of our knowledge, only one PCARS result has been published on single crystals of the 1111 family, namely on F-doped Sm-1111 [68]. There, Karpinski *et al.* reported AR spectra, measured by injecting the current along the ab -plane, that were fitted by two nodeless gaps, in good agreement with other results obtained on polycrystals by Daghero *et al.* [56] (panel b). On the other hand, early measurements by Chen *et al.* [55] were interpreted in terms of a single BCS gap (panel a), i.e. isotropic, independent of energy and with a $2\Delta / k_B T_c$ ratio of about 3.5 and temperature behavior

http://dx.doi.org/10.5772/59587

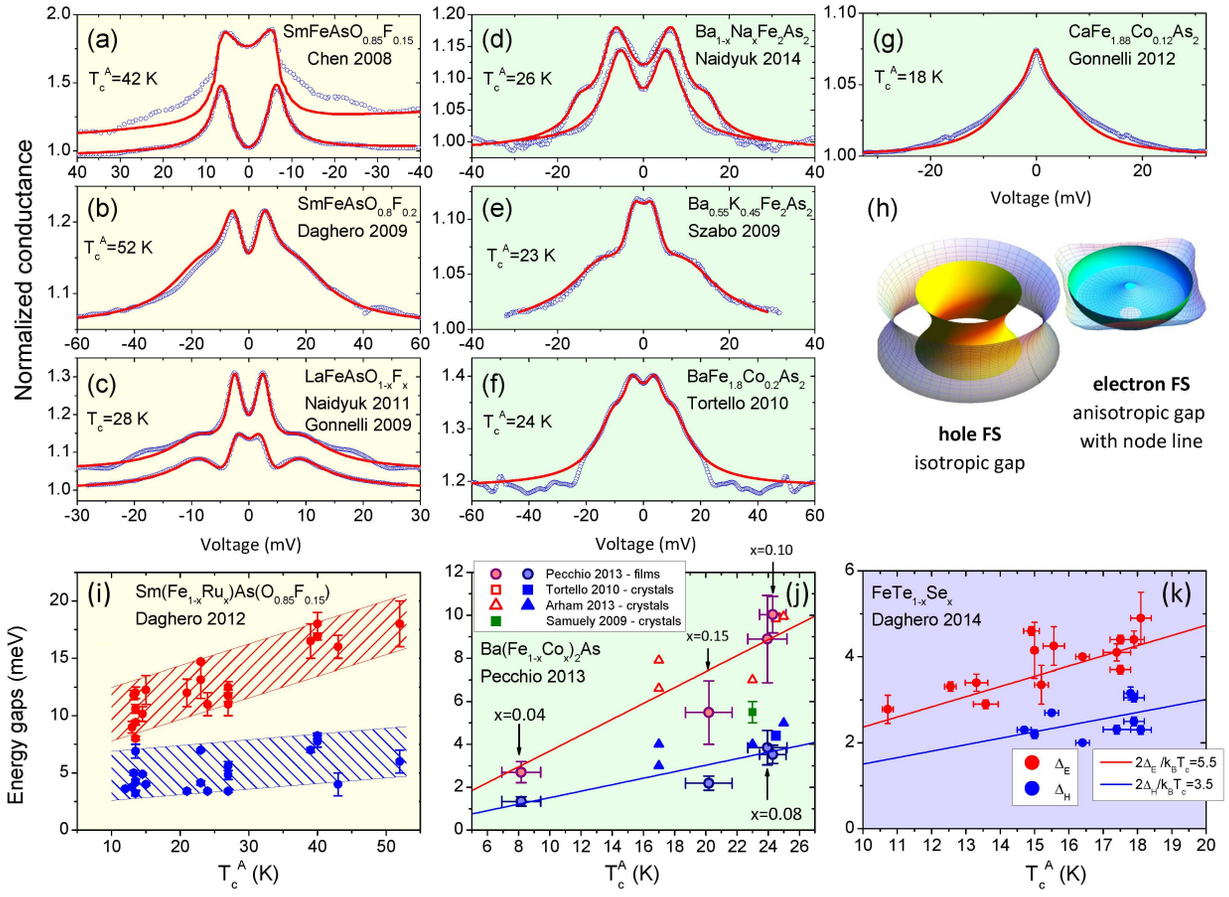

Figure 4. (a,b) Symbols: examples of PCARS spectra in polycrystalline Sm-1111 (from refs. [55] and [56]) with the relevant fit (lines), with a single isotropic gap (a) and two isotropic gaps (b). (c) PCARS spectra in La-1111 polycrystals (from [57]) and films (from [58]) with the relevant fit with two isotropic gaps as suggested in [27]. (d) PCARS spectra in $Ba_{1-x}Na_xFe_2As_2$ single crystals [59] fitted with either two (upper curves) or one (lower curve) isotropic gap. Whether the shoulders at $\simeq 15$ meV are due to a second gap is actually doubtful. (e,f) PCARS spectra in K-doped (from [60]) and Co-doped Ba-122 (from [61]) single crystals with the fit with two isotropic gaps. (g) An in-plane example of PCARS spectra in Co-doped Ca-122 crystals that prove the presence of nodes in the gap, with the relevant 3D-BTK fit with two gaps, of which one has a horizontal line of nodes. The model FS and the gap structure used in the 3D BTK model are shown in (h) as matt and gridded surfaces. (i) Effect of isovalent substitution (Ru in the Fe site) on the gaps of Sm-1111. The gaps are reported as a function of T_c^A (from [62]). (j) T_c^Adependence of the gaps in $Ba(Fe_{1-x}Co_x)_2As_2$ films with different x (indicated by labels) compared to other PCARS results [61, 63, 64]. In the UD regime $(x \leq 10)$ the gap ratios $2\Delta_i / k_B T_c$ are 3.52 and 9 (lines), in the OD regime they decrease. (k) Gaps of $FeTe_{1-x}Se_x$ films with $x = 0.3$, 0.4 and 0.5 as a function of T_c^A (from [65]). The gap ratios $2\Delta_i / k_B T_c$ are constant (solid lines). In (i, j, k) the gaps were obtained by fitting the PCARS spectra with two isotropic gaps.

as in the original BCS paper [6]. Daghero *et al.* [56] reported a rather large scattering of the values for the large OP, which is also one of the arguments invoked to argue that the large gap is actually not a gap. However, there can be other explanations. First, the features associated to the larger gap are often less defined in energy [58] and may not give rise to double maxima but show up rather as " shoulders" in the conductance. Second, it is actually possible that more than two gaps are present in these compounds, and that PCARS is unable to discriminate between the (multiple) large ones. It turns indeed out that the minimal theoretical model to reproduce the

experimental gaps, within the Eliashberg-like theory assuming a spin-fluctuations-mediated mechanism, has to take into account at least three bands [69]. On the other hand, a fit of the experimental spectra with a three-gap model could easily be meaningless because of the much too high number of free parameters. Therefore, a two-gap model is generally used and the noticeable scattering of the large gap values in, for instance, ref. [56] has most probably to be ascribed to the fact that more than two gaps are picked up, as a whole, by different PCARS spectra. PCARS was also performed on 1111 thin films [58] where the large gap was difficult to resolve. There, this fact was mainly explained by a possible large interband scattering that smears out the larger gap features, even though it has been shown that a two-gap model could indeed fit the data rather well [27], as reported in the upper curve of panel c.

The possibility to grow large single crystals of the 122 family made these materials the most studied ones among FeBS, also as far as PCARS is concerned (Figure 4d-h and j). Multi-gap, nodeless superconductivity was reported for K-, Co- and Ni-doped Ba 122 crystals [60, 61, 70] (see Figures 4e, f and 5a, respectively). On the other hand, only one gap has been clearly resolved, at least up to now, in $Ba_{1-x}Na_xFe_2As_2$ ($x=0.25$) [59] (Figure 4d, lower curve) and $SrFe_{1.74}Co_{0.26}As_2$ [71]. In particular, additional structures were observed in $Ba_{1-x}Na_xFe_2As_2$ at higher energies that, when fitted as a second gap, gave an unrealistically large $2\Delta/k_BT_c$ value, ≈ 15, (panel d, upper curve). By the way, similar features have recently been reported also for Fe(Te,Se) thin films and interpreted as electron-boson interaction features [65]. PCS results in Na-doped Sr 122 didn't show AR features but V-shaped spectra, that were interpreted in terms of possible electron scattering from magnetic order [72].

In some cases, depending on the details of the pairing interaction, the structure of the order parameter can become, within the s -wave symmetry, anisotropic and feature gap minima or line nodes where the OP changes sign on a FS sheet, either hole- or electron-like [73, 74, 16]. In these situations, the use of the 3D BTK model that takes into account the actual shape of the Fermi surface, even though approximated by a suitable parametric function, can be unavoidable in order to catch these finer details of the gap structure. Horizontal line nodes have indeed been observed by PCARS in the $CaFe_2As_2$ compound under pressure [36]. The point contact spectra were very well fitted by the 3D BTK model and results theoretically supported both by calculations of the electronic structure (within the Density Functional Theory) and of the gap structure (within a Random Phase Approximation approach in a ten-orbital model), thus giving a self-consistent experimental/theoretical picture of the OP in this compound. A similar gap structure (but more anisotropic) is inferred also by PCARS measurements on Co-doped $CaFe_2As_2$ where the spectra can be fitted by the 3D BTK model taking into account the FS topology, as shown in Figure 4g and h.

As for the 111 family, multiple nodeless gaps were reported for Co-doped NaFeAs [75] while only one nodeless gap was observed by PCARS measurements on LiFeAs [76].

Multiband superconductivity was also reported for Fe(Te,Se) films. In this case, the small gap was the most difficult to resolve [65]. Ref. [65] also reported the evolution of the two gaps as a function of T_c, which increases with increasing the Se content from $x=0.3$ to $x=0.5$. The two gaps have been found to decrease rather monotonically with the critical temperature of the PCARS junctions (see Figure 4k) and since their gap ratios remain constant, this means that

http://dx.doi.org/10.5772/59587

the amplitudes of the gaps perfectly scale with T_c, i.e. if plotted as a function of doping they would mimic the behavior of the critical temperature. The only caveat in this respect is that the values of the gap amplitudes in each point contact are related to the *local* T_c^A of the contact rather than to bulk properties (such as the average doping or the T_c measured by electrical transport).

There are not so many examples in the literature, up to now, of systematic PCARS studies of the evolution of the OPs as a function of doping or disorder. Panels i and j report other examples of energy gaps as a function of the critical temperature, when the latter is modulated by means of chemical substitutions, either isovalent (Ru for Fe) in optimally F-doped Sm-1111 polycrystals (i), or aliovalent (Co for Fe) in Ba-122 thin films (j). This kind of studies might be very important in the attempt of unraveling the symmetry and structure of the OPs since, in some cases, a change of symmetry has been theoretically predicted when changing some lattice parameters [77].

Interband interference effects and sub-gap bound states in the Andreev spectra have been theoretically predicted as a consequence of an $s_{\pm}$ gap structure [78]. These features though, have not been reported in any experimental PCARS study up to now. Possibly they may be washed out by broadening effects or may occur at particular conditions of the model that make them hardly distinguishable from a more stardard s_{++} BTK conductance. According to this model, these interference effects indeed depend on a free parameter, αwhose value has not been predicted theoretically and changes dramatically the shape of the spectra. However, interference effects on the BTK conductance due to a sign-changing s -wave OP in multi-band systems have also been recently calculated [79] by using the quantum waveguides theory. Simple analytical formulas were obtained that depend on the ratios of the Fermi velocities of the normal metal and the superconducting bands and could be easily compared to experimental spectra, possibly helping to catch signatures of a sign-changing OP.

4.2.1. Electron-boson interaction in FeBS

As already noticed in 2.2, in case of moderate- to strong-coupling regime, the energy dependence of the OP can give rise to EBI features in the conductance spectra that can be better singled out by taking the sign-changed second derivative of the I-V characteristic. These features can give important information regarding the pairing mechanism because they indicate that electrons are actually interacting with some fundamental excitation of the material under study. EBI characteristics were reported for Co- and Ni-doped (Figure 5a) Ba-122 single crystals [61, 70]. In both Co- and Ni- doping the main EBI feature showed up at $E_p \approx \Delta_{max} + \Omega_b$ (panel b). The characteristic bosonic energy, $\Omega_b$was very similar to the spin-resonance energy observed in neutron scattering experiments on the same compound [80].

Moreover, $\Omega_b$decreased as a function of temperature (panel c), a behavior incompatible with a phononic interaction whose energy is expected to be temperature-independent. As reported in section 3.2, it is possible to include the energy-dependent expression for the gap in the BTK model and compare the result with the experimental normalized conductance. Panel d reports

an example for an optimally F-doped Sm-1111 polycrystalline sample [27] where it is shown that, besides reproducing the two energy gaps, the theoretical conductance can reproduce very well the EBI feature at about 40 meV and the shape of the high-energy tails, but not the one at 25 meV. This might be due to finer details of the bosonic spectral function that was modeled by a Lorentzian function in the theoretical analysis. It is also worth reminding in this regard that, as shown in ref. [27], in multiband systems the EBI features don't necessarily occur at energies of the order of $\Delta_{max} + \Omega_b$, but a detailed calculation of the energy dependence of the gap is desirable. Similar results have also been recently reported for Fe(Te,Se) thin films [65]. The presence of EBI features at these energies and the fact that the experimental gaps can be reproduced within the Eliashberg-like model, by using a spectral function with Lorentzian shape whose characteristic energy is Ω_b [27, 61, 65], strongly support a spin-fluctuations-mediated mechanism of superconductivity in FeBS.

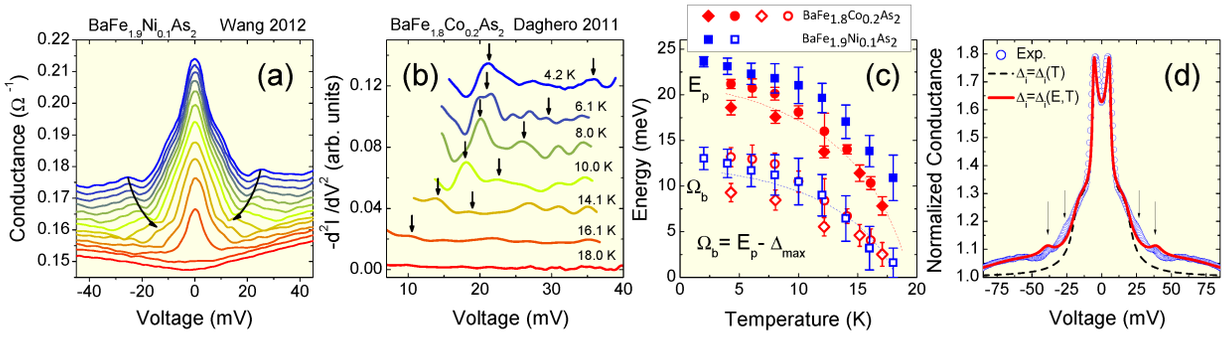

Figure 5. (a) Temperature dependence of the raw conductance curves (shifted downward for clarity) obtained from a *c* -axis Ag/$BaFe_{1.9}Ni_{0.1}As_2$ junction. Temperatures range from 2 K (upper one) to 20 K with a step of 2 K. The last curve is measured at 21 K. Arrows indicate the temperature evolution of the EBI features occurring at energies of about $E_p(T) \approx \Delta_{max}(T) + \Omega_b(T)$ where $\Omega_b(T)$ is the characteristic bosonic energy (from [70]). (b) Temperature dependence of the sign-changed second derivative of the $I-V$ characteristics in the $BaFe_{1.5}Co_{0.2}As_2$ point-contact junctions (from [27, 61]). (c) Temperature evolution of E_p and Ω_b in $BaFe_{1.9}Ni_{0.1}As_2$ (squares) and $BaFe_{1.8}Co_{0.2}As_2$ (diamonds and circles) single crystals as reported in refs. [70, 61]. (d) Normalized conductance curve (circles) measured from a Ag/$SmFeAsO_{0.8}F_{0.2}$ point-contact junction. The dashed line is a BTK fit to the experiment, obtained using energy-independent values for the gaps (Δ_1=6.0meV and Δ_2=19.5 meV). The solid line is a theoretical curve obtained by introducing in the BTK model the energy-dependent gap functions calculated within the three-band Eliashberg theory whose values are Δ_1=17.23 meV, Δ_2=6.03meV and Δ_3=−19.56 meV (from [27]).

EBI features have also been observed in the normal state of KFe_2As_2 [81]. The d^2V/dI^2 characteristics showed a peak at about 20 meV, while were featureless at higher and lower energies. The results were interpreted on the basis of charge excitations (excitonic-like), a non-phononic and non-magnetic type of interaction never observed before in PCS spectra. The authors argued that the manifestation of the EBI features in PCS spectra on these compounds has been possible thanks to an electron mass renormalization larger than in many metallic systems.

Finally, a conductance enhancement around zero bias has been reported in the PCS spectra in the normal state of several FeBS, and interpreted as being tied to interactions with orbital

http://dx.doi.org/10.5772/59587

fluctuations, thus providing indication of electronic nematicity [82]. It has also been argued that such excess density of states can be actually picked up by PCS thanks to the presence of non-negligible electronic correlations in the studied materials [83].

5. Conclusion

The BCS theory (and, when necessary, its generalizations to the anisotropic and multiband case) was able to give a satisfactory description of conventional superconductors in terms of electron-phonon coupling, and the Eliashberg theory can better describe them when the coupling is stronger. Both theories can, in principle, be generalized to any pairing glue. In electron-phonon superconductors, the OP parameter is generally single and isotropic but more complex anisotropies [84] or multi-band scenarios [30] have been observed as well.

However, superconductivity in unconventional HTSC cannot be explained by the same pairing mechanism. In this regard, the knowledge of the number, amplitude, symmetry and structure of their OP is essential in order to satisfactorily describe their superconducting state and pairing mechanism. As a matter of fact, this task turned out to be tremendously more complicated and challenging than for conventional superconductors.

Thanks to the Andreev reflection process, PCARS has been able to address this issue to a good extent. The complicated scenarios proposed for HTSC pushed the development of models of increasing complexity that certainly helped to achieve a more accurate analysis of the experimental data and to catch important details regarding the OP in HTSC. At the same time, as we have seen by mainly focusing on the results of PCS in the Andreev reflection regime, several issues are still open in this field.

There is a general consensus that several cuprates have a dominant d -wave symmetry. However, for many of them additional components of the OP (mixed symmetries) were reported, which sometimes appeared to set in only at certain doping levels. Their origin still needs to be clarified as well as the pairing mechanism and its relation to the OP. Moreover, sample- or surface-related issues may also play a role.

Often, PCARS results turned out to be different from those obtained by ARPES or STM. Although some of these discrepancies still have to be reconciled, on the other hand they sometimes gave complementary information because, for example, PCARS is sensitive to the phase-coherent pairs while STM probes the single-particle states. Contrasting results have been obtained for electron-doped cuprates as well, some of which also considerably differ from those observed in the hole-doped ones, even suggesting that some of them are weak-coupling BCS (one isotropic gap with $2\Delta/k_BT_c \approx 3.5$) superconductors. Therefore, a consistent generalization between the two types of cuprates is very far from being achieved.

Most FeBS certainly feature multiple superconducting bands and gaps and a more general picture of the present state of the art can be achieved. Nevertheless, a precise knowledge of

the main features of the OPs is still lacking. Even the knowledge of tiny differences in their structure might be important in order to unravel their pairing glue and, apparently, some new compounds seem to pose into question some of the most successful theoretical models. In particular, distinguishing between an $s_{\pm}$ - and s_{++} -wave structure of the OP is turning out to be a conundrum and unambiguous phase-sensitive experiments on single crystals have not been performed yet in FeBS. Several have been proposed though, and experiments making use of point contacts may also be very useful in this regard [85].

PCARS is not sensitive to the phase of the OP and, unlike in cuprates, interference effects (that would be expected only for the $s_{\pm}$ -wave structure) have not been clearly observed yet. Their (possible) observation is indeed complicated by the particular electronic structure and by the similarity between the two main OP structures proposed. However, theoretical models of increasing complexity are being developed that may be able to detect signatures of a possible sign change of the OP in FeBS. For the time being, the use of the 3D BTK model turned out to be very useful and helped to catch, even though somehow indirectly, finer details of the structure of the OPs, like gap anisotropies or line nodes, thus putting more stringent constraints on the present theoretical predictions. The study of the dependence of the OPs as a function of doping or disorder in FeBS might be very important also because the few PCARS results reported up to now do not show the puzzling behavior obtained in many PCARS studies on cuprates.

Moreover, the possibility to detect electron-boson interaction features in the point contact characteristics may be crucial in clarifying the pairing mechanism as not only EBI features indicate the presence of some fundamental excitation, but more specifically show their interaction with the electrons in the material.

FeBS feature many differences in comparison with cuprates and, as we have briefly mentioned, PCARS methods and models are evolving for better investigating the former class of compounds. Also, PCARS results obtained up to now, although far from being conclusive, seem less puzzling than for cuprates. Therefore, it is hoped that the progress achieved up to now and the new methods developed for investigating FeBS by PCARS may at least aid shedding light on cuprates as well. A more general and complete picture of HTSC and a clarification of their relevant pairing mechanism(s) is indeed a major objective of the present research in the field of solid state physics. The achievement of this goal would hopefully pave the way for the discovery of new materials with higher T_c and better properties, especially in view of the current applications of superconductivity and of the potentially revolutionary ones that may be realized with new high- T_c superconductors.

Acknowledgements

The authors would like to warmly thank R.S. Gonnelli and G.A. Ummarino for useful discussions and for perusing the manuscript. The results of our group shown in this chapter, were obtained also thanks to the contributions of V.A. Stepanov and P. Pecchio.

http://dx.doi.org/10.5772/59587

Author details

M. Tortello* and D. Daghero

*Address all correspondence to: mauro.tortello@polito.it

Dipartimento di Scienza Applicata e Tecnologia (DISAT), Politecnico di Torino, Torino, Italy

References

[1] J. G. Bednorz and K. A. Müller. Possible high T_c superconductivity in the Ba-La-Cu-O system. *Z. Physik, B*, 64:189, 1986.

[2] VV. AA. Celebratory issue on high T_c superconductors. *Nature Phys.*, 2, 2006.

[3] Y. Kamihara, T. Watanabe, M. Hirano, and H. Hosono. Iron-based layered superconductor $LaO_{1-x}F_xFeAs$ (x = 0.05-0.12) with T_c = 26 K. *J. Am. Chem. Soc.*, 130:3296, 2008.

[4] Z. A. Ren, J. Yang, W. Lu, W. Yi, X. L. Shen, Z. C. Li, G. C. Che, X. L. Dong, L. L. Sun, F. Zhou, and Z. X. Zhao. Superconductivity in the iron-based F-doped layered quaternary compound $NdO_{1-x}F_xFeAs$. *Europhys. Lett.*, 82:57002, 2008.

[5] A. M. Gabovich and V. I. Kuznetsov. What do we mean when using the acronym BCS? The Bardeen Cooper Schrieffer theory of superconductivity. *Eur. J. Phys.*, 34:371, 2013.

[6] J. Bardeen, L. N. Cooper, and J. R. Schrieffer. Theory of superconductivity. *Phys. Rev.*, 108:1175–204, 1957.

[7] J. R. Waldram. *Superconductivity of metals and cuprates*. Institute of Physics Publishing, 1996.

[8] I. I. Mazin and V. P. Antropov. Electronic structure, electron–phonon coupling, and multiband effects in MgB_2. *Physica C*, 385:49, 2003.

[9] R. A. Klemm, C. T. Rieck, and K. Scharnberg. Order-parameter symmetries in high-temperature superconductors. *Phys. Rev. B*, 61:5913, 2000.

[10] C. C. Tsuei and J. R. Kirtley. Pairing symmetry in cuprate superconductors. *Rev. Mod. Phys.*, 72:969, 2000.

[11] H. Suhl, B. T. Matthias, and L. R. Walker. Bardeen-Cooper-Schrieffer theory of superconductivity in the case of overlapping bands. *Phys. Rev. Lett.*, 3:552, 1959.

[12] V.A. Moskalenko. Superconductivity of metals with overlapping energy bands. *Fiz. Met. Metalloved. (Phys. Met. Metallogr. (URSS))*, 4:503, 1959.

[13] A. A. Golubov and I. I. Mazin. Sign reversal of the order parameter in *s*-wave superconductors. *Physica C*, 243:153, 1995.

[14] I. I. Mazin, D. J. Singh, M. D. Johannes, and M. H. Du. Unconventional superconductivity with a sign reversal in the order parameter of $LaFeAsO_{1-x}F_x$. *Phys. Rev. Lett.*, 101:057003, 2008.

[15] L. Boeri, O. V. Dolgov, and A. A. Golubov. Is $LaFeAsO_{1-x}F_x$ an electron-phonon superconductor? *Phys. Rev. Lett.*, 101:026403, 2008.

[16] P. J. Hirschfeld, M. M. Korshunov, and I. I. Mazin. Gap symmetry and structure of Fe-based superconductors. *Rep. Prog. Phys.*, 74:124508, 2011.

[17] G. M. Eliashberg. Interactions between electrons and lattice vibrations in a superconductor. *Sov. Phys. JETP*, 11:696, 1963.

[18] J.P. Carbotte. Properties of boson-exchange superconductors. *Rev. Mod. Phys.*, 62:1027, 1990.

[19] G. A. Ummarino. *Emergent Phenomena in Correlated Matter*, volume 3, chapter Eliashberg theory, pages 13.1–13.36. Forschungszentrum Julich Gmbh and Institute for Advanced Simulations, 2013.

[20] H. J. Choi, D. Roundy, H. Sun, M. L. Cohen, and S. G. Louie. The origin of the anomalous superconducting properties of MgB_2. *Nature*, 418:758–760, 2002.

[21] P.B. Allen. Fermi-surface harmonics: A general method for nonspherical problems. Application to Boltzmann and Eliashberg equations. *Phys. Rev. B*, 13:1416, 1976.

[22] P.B. Allen. New method for solving Boltzmann's equation for electrons in metals. *Phys. Rev. B*, 17:3725, 1978.

[23] I. K. Yanson. Nonlinear effects in the electric conductivity of point junctions and electron-phonon interaction in normal metals. *Sov. Phys. JETP*, 39:506–513, 1974.

[24] Yu. G. Naidyuk and I. K. Yanson. *Point-Contact Spectroscopy*, volume 145 of *Springer Series in Solid-State Sciences*. Springer, 2004.

[25] G. E. Blonder, M. Tinkham, and T. M. Klapwijk. Transition from metallic to tunneling regimes in superconducting microconstrictions: Excess current, charge imbalance, and supercurrent. *Phys. Rev. B*, 25:4515, 1982.

[26] D. Daghero and R.S. Gonnelli. Probing multiband superconductivity by point-contact spectroscopy. *Supercond. Sci. Technol.*, 23:043001, 2010.

[27] D. Daghero, M. Tortello, G.A. Ummarino, and R. S. Gonnelli. Directional point-contact Andreev-reflection spectroscopy of Fe-based superconductors: Fermi surface topology, gap symmetry, and electron-boson interaction. *Rep. Prog. Phys.*, 74:124509, 2011.

http://dx.doi.org/10.5772/59587

[28] G. Deutscher. Andreev-Saint-James reflections: A probe of cuprate superconductors. *Rev. Mod. Phys.*, 77:109–35, 2005.

[29] D. Daghero, M. Tortello, P. Pecchio, V. A. Stepanov, and R. S. Gonnelli. Point-contact Andreev-reflection spectroscopy in anisotropic superconductors: the importance of directionality. *Low Temp. Phys.*, 39:261, 2013.

[30] R. S. Gonnelli, D. Daghero, G. A. Ummarino, V. A. Stepanov, J. Jun, S. M. Kazakov, and J. Karpinski. Direct evidence for two-band superconductivity in MgB_2 single crystal from directional point-contact spectroscopy in magnetic field. *Phys. Rev. Lett.*, 89:247004, 2002.

[31] A. Andreev. Thermal conductivity of the intermediate state of superconductors. *Zh. Eksp. Teor. Fiz.*, 46:1823, 1964. Engl. Transl. Sov. Phys.-JETP 19, 1228 (1974).

[32] G.E. Blonder and M. Tinkham. Metallic to tunneling transition in Cu-Nb point contacts. *Phys. Rev. B*, 27:112, 1983.

[33] R. C. Dynes, V. Narayanamurti, and J. P. Garno. Direct measurement of quasiparticle-lifetime broadening in a strong-coupled superconductor. *Phys. Rev. Lett.*, 41:1509, 1978.

[34] A. Plecenik, M. Grajcar, Š. Beňaňka, P. Seidel, and A. Pfuch. Finite quasiparticle-lifetime effects in the differential condutance of $Bi_2Sr_2CaCu_2O_y$/Au junctions. *Phys. Rev. B*, 49:10016, 1994.

[35] S. Kashiwaya, Y. Tanaka, M. Koyanagi, and K. Kajimura. Theory for tunneling spectroscopy of anisotropic superconductors. *Phys. Rev. B*, 53:2667, 1996.

[36] R. S. Gonnelli, D. Daghero, M. Tortello, G. A. Ummarino, Z. Bukowski, J. Karpinski, P. G. Reuvekamp, R. K. Kremer, G. Profeta, K. Suzuki and K. Kuroki Fermi-surface topological phase transition and horizontal order parameter nodes in $CaFe_2As_2$ under pressure. Preprint at arXiv:1406.5623 [cond-mat.supr-con], 2014.

[37] A. Brinkman, A. A. Golubov, H. Rogalla, O. V. Dolgov, J. Kortus, Y. Kong, O. Jepsen, and O. K. Andersen. Multiband model for tunneling in MgB_2 junctions. *Phys. Rev. B*, 65:180517, 2002.

[38] I. I. Mazin. How to define and calculate the degree of spin polarization in ferromagnets. *Phys. Rev. Lett.*, 83:1427, 1999.

[39] J. Y. T. Wei, N.-C. Yeh, D. F. Garrigus, and M. Strasik. Directional Tunneling and Andreev Reflection on $YBa_2Cu_3O_{7-}$ Single Crystals: Predominance of d-Wave Pairing Symmetry Verified with the Generalized Blonder, Tinkham, and Klapwijk Theory. *Phys. Rev. Lett.*, 81:2542, 1998.

[40] G. Deutscher and R. Maynard. *The Gap Symmetry and Fluctuations in High-T_c Superconductors*, chapter From the Andreev reflection to the Sharvin contact conductance, pages 503–510. NATO Science Series: B. Kluwer Academic Publishers, 2002.

[41] S. Kashiwaya and Y. Tanaka. Tunnelling effects on surface bound states in unconventional superconductors. *Rep. Prog. Phys.*, 63:1641-1724, 2000.

[42] N. P. Armitage, P. Fournier, and R. L. Greene. Progress and perspectives on electron-doped cuprates. *Rev. Mod. Phys.*, 82:2421, 2010.

[43] A. Kohen, G. Leibovitch, and G. Deutscher. Andreev Reflections on $Y_{1-x}Cu_x$ Ba_2O_{7-}: Evidence for an Unusual Proximity Effect. *Phys. Rev. Lett.*, 90:207005, 2003.

[44] M. Fogelström, D. Rainer, and J. A. Sauls. Tunneling into Current-Carrying Surface States of High- Tc Superconductors. *Phys. Rev. Lett.*, 79:281, 1997.

[45] M. Covington, M. Aprili, E. Paraoanu, L. H. Greene, F. Xu, J. Zhu, and C. A. Mirkin. Observation of Surface-Induced Broken Time-Reversal Symmetry in $YBa_2Cu_3O_7$ Tunnel Junctions. *Phys. Rev. Lett.*, 79:277, 1997.

[46] A. Sharoni, G. Koren, and O. Millo. Correlation of tunneling spectra with surface nanomorphology and doping in thin $YBa_2Cu_3O_{7-}$ films. *Europhys. Lett.*, 54:675, 2001.

[47] R. Beck, Y. Dagan, A. Milner, A. Gerber, and G. Deutscher. Order-parameter-node removal in the d-wave superconductor $YBa_2Cu_3O_{7-x}$ in a magnetic field. *Phys. Rev. B*, 69:144506, 2004.

[48] G Deutscher, N. Achsaf, D. Goldschmidt, A. Revcolevschi, and A. Vietkine. Andreev reflections from $La_{2x}Sr_xCuO_4$ single crystals. *Physica C*, 282-287:140, 1997.

[49] R. S. Gonnelli, A. Calzolari, D. Daghero, L. Natale, G. A. Ummarino, V. A. Stepanov, and M. Ferretti. Evidence for pseudogap and phase-coherence gap separation by Andreev reflection experiments in $Au/La_{2-x}Sr_xCuO_4$ point-contact junctions. *Eur. Phys. J. B*, 22:411, 2001.

[50] D. Daghero, R. S. Gonnelli, G. A. Ummarino, and V. A. Stepanov. Possible *d+id* scenario in $La_{2-x}Sr_xCuO_4$ by point-contact measurements. *Int. J. Mod. Phys.*, 17:649, 2003.

[51] L. Shan, Y. Huang, H. Gao, Y. Wang, S. L. Li, P. C. Dai, F. Zhou, J. W. Xiong, W. X. Ti, and H. H. Wen. Distinct pairing symmetries in $Nd_{1.85}Ce_{0.15}CuO_{4-y}$ and $La_{1.89}Sr_{0.11}CuO_4$ single crystals: Evidence from comparative tunneling measurements. *Phys. Rev. B*, 72:144506, 2005.

[52] A. Biswas, P. Fournier, M. M. Qazilbash, V. N. Smolyaninova, H. Balci, and R. L. Greene. Evidence of a *d*- to *s*-Wave Pairing Symmetry Transition in the Electron-Doped Cuprate Superconductor $Pr_{2-x}Ce_xCuO_4$. *Phys. Rev. Lett.*, 88:207004, 2002.

[53] Y. Dagan, R. Beck, and R. L. Greene. Dirty Superconductivity in the Electron-Doped Cuprate $Pr_{2-x}Ce_xCuO_{4-}$: Tunneling Study. *Phys. Rev. Lett.*, 99:147004, 2007.

[54] J. Paglione and R. L. Greene. High-temperature superconductivity in iron-based materials. *Nature Phys.*, 6:645–58, 2010.

[55] T. Y. Chen, Z. Tesanovic, R. H. Liu, X. H. Chen, and C. L. Chien. A BSC-like gap in the superconductor $SmFeAsO_{0.85}F_{0.15}$. *Nature (London)*, 453:761, 2008.

[56] D. Daghero, M. Tortello, R. S. Gonnelli, V. A. Stepanov, N. D. Zhigadlo, and J. Karpinski. Evidence for two-gap nodeless superconductivity in $SmFeAsO_{1-x}F_x$ from point-contact Andreev-reflection spectroscopy. *Phys. Rev. B*, 80:060502(R), 2009.

[57] R. S. Gonnelli, D. Daghero, M. Tortello, G. A. Ummarino, V. A. Stepanov, J. S. Kim, and R. K. Kremer. Coexistence of two order parameters and a pseudogaplike feature in the iron-based superconductor $LaFeAsO_{1-x}F_x$. *Phys. Rev. B*, 79:184526, 2009.

[58] Yu. G. Naidyuk, O. E. Kvitnitskaya, I. K. Yanson, G. Fuchs, S. Haindl, M. Kidszun, L. Schultz, and B. Holzapfel. Point-contact study of $ReFeAs_{1-x}F_x$ (Re=La, Sm) superconducting films. *Supercond. Sci. Technol.*, 24:065010, 2011.

[59] Yu. G. Naidyuk, O. E. Kvitnitskaya, S. Aswartham, G. Fuchs, K. Nenkov, and S. Wurmehl. Exploring point-contact spectra of $Ba_{1-x}Na_xFe_2As_2$ in the normal and superconducting states. *Phys. Rev. B*, 84:094516, 2011.

[60] P. Szabó, Z. Pribulová, G. Pristáš, S. L. Bud'ko, P. C. Canfield, and P. Samuely. Evidence for two-gap superconductivity in $Ba_{0.55}K_{0.45}Fe_2As_2$ from directional point-contact Andreev-reflection spectroscopy. *Phys. Rev. B*, 79:012503, 2009.

[61] M. Tortello, D. Daghero, G. A. Ummarino, V. A. Stepanov, J. Jiang, J. D. Weiss, E. E. Hellstrom, and R. S. Gonnelli. Multigap Superconductivity and Strong Electron-Boson Coupling in Fe-Based Superconductors: A Point-Contact Andreev-Reflection Study of $Ba(Fe_{1-x}Co_x)_2As_2$ Single Crystals. *Phys. Rev. Lett.*, 105:237002, 2010.

[62] D. Daghero, M. Tortello, G.A. Ummarino, V. A. Stepanov, F. Bernardini, M. Tropeano, M. Putti, and R. S. Gonnelli. Effects of isoelectronic Ru substitution at the Fe site on the energy gaps of optimally F-doped SmFeAsO. *Supercond. Sci. Technol.*, 25:084012, 2012.

[63] H. Z. Arham, C. R. Hunt, J. Gillett, S. D. Das, S. E. Sebastian, D. Y. Chung, M. G. Kanatzidis, and L. H. Greene. Andreev reflection like enhancement above bulk T_c in electron underdoped iron arsenides. Preprint at arXiv:1307.1908 [cond-mat.supr-con], 2013.

[64] P. Samuely, Z. Pribulová, P. Szabó, G. Pristáš, S. L. Bud'ko, and P. C. Canfield. Point contact Andreev reflection spectroscopy of superconducting energy gaps in 122-type family of iron pnictides. *Physica C*, 469:507, 2009.

[65] D. Daghero, P. Pecchio, G.A. Ummarino, F. Nabeshima, Y. Imai, A. Maeda, I. Tsukada, Komiya S., and R. S. Gonnelli. Point-contact Andreev-reflection spectroscopy in Fe(Te,Se) films: multiband superconductivity and electron-boson coupling. *Supercond. Sci. Technol.*, 27:124014, 2014.

[66] R. M. Fernandes, A. V. Chubukov, and J. Schmalian. What drives nematic order in iron-based superconductors? *Nature Phys.*, 10:97–104, 2014.

[67] H Miao, P. Richard, Y. Tanaka, K. Nakayama, T. Qian, K. Umezawa, T. Sato, Y.-M. Xu, Y. B. Shi, N. Xu, X.-P. Wang, P. Zhang, H.-B. Yang, Z.-J. Xu, J. S. Wen, G.-D. Gu, X. Dai, J.-P. Hu, T. Takahashi, and H. Ding. Isotropic superconducting gaps with enhanced pairing on electron Fermi surfaces in $FeTe_{0.55}Se_{0.45}$. *Phys. Rev. B*, 85:094506, 2012.

[68] J. Karpinski, N. Zhigadlo, S. Katrych, Z. Bukowski, P. Moll, S. Weyeneth, H. Keller, R. Puzniak, M. Tortello, D. Daghero, R. S. Gonnelli, I. Maggio-Aprile, Y. Fasano, Ø. Fischer, K. Rogacki, and B. Batlogg. Single crystals of $LnFeAsO_{1-x}F_x$ (Ln = La, Pr, Nd, Sm, Gd) and $Ba_{1-x}Rb_xFe_2As_2$: Growth, structure and superconducting properties. *Physica C*, 469:370, 2009.

[69] G. A. Ummarino, M. Tortello, D. Daghero, and R. S. Gonnelli. Three-band *s*± Eliashberg theory and the superconducting gaps of iron pnictides. *Phys. Rev. B*, 80:172503–1–4, 2009.

[70] Z.-S. Wang, Z.-Yu Wang, H.-Q. Luo, X.-Ye Lu, J. Zhu, C.-H. Li, L. Shan, H. Yang, H.-H. Wen, and C. Ren. Electron-boson coupling and two superconducting gaps in optimally electron-doped $BaFe_{1.9}Ni_{0.1}As_2$ single crystals. *Phys. Rev. B*, 86:060508(R), 2012.

[71] X. Zhang, Y. S. Oh, Y. Liu, L. Yan, S.R. Saha, N. P. Butch, K. Kirshenbaum, K. H. Kim, J. Paglione, R. L. Greene, and I. Takeuchi. Evidence of a universal and isotropic $2\Delta/k_b$ T_c ratio in 122-type iron pnictide superconductors over a wide doping range. *Phys. Rev. B*, 82:020515(R), 2010.

[72] X. Lu, W. K. Park, H. Q. Yuan, G. F. Chen, G. L. Luo, N. L. Wang, A. S. Sefat, M. A. McGuire, R. Jin, B. C. Sales, D. Mandrus, J. Gillett, S. E. Sebastian, and L. H. Greene. Point-contact spectroscopic studies on normal and superconducting AFe_2As_2-type iron pnictide single crystals. *Supercond. Sci. Technol.*, 23:054009, 2010.

[73] I. I. Mazin, T. P. Devereaux, J. G. Analytis, Jiun-Haw Chu, I. R. Fisher, B. Muschler, and R. Hackl. Pinpointing gap minima in $Ba(Fe_{0.94}Co_{0.06})_2As_2$ via band-structure calculations and electronic raman scattering. *Phys. Rev. B*, 82:180502(R), 2010.

[74] K. Suzuki, H. Usui, and K. Kuroki. Possible three dimensional nodes in the *s*± superconducting gap of $BaFe_2(As_{1-x}P_2)_2$. *J. Phys. Soc. Jpn.*, 80:013710, 2011.

[75] H. Z. Arham, D. E. Bugaris, D. Y. Chung, M. G. Kanatzidis, and L. H. Greene. Point contact spectroscopy in the superconducting and normal state of $NaFe_{1-x}Co_xAs$. Preprint at arXiv:1406.0038v1 [cond-mat.supr-con], 2014.

[76] X. Zhang, B. Lee, S. Khim, K.H. Kim, R. L. Greene, and I. Takeuchi. Probing the order parameter of superconducting LiFeAs using Pb/LiFeAs and Au/LiFeAs point-contact spectroscopy. *Phys. Rev. B*, 85:094521, 2012.

[77] K. Kuroki, H. Usui, S. Onari, R. Arita, and H. Aoki. Pnictogen height as a possible switch between high- T_c nodeless and low-T_c nodal pairings in the iron-based superconductors. *Phys. Rev. B*, 79:224511, 2009.

[78] A. A. Golubov, A Brinkman, Y. Tanaka, I. I. Mazin, and O. V. Dolgov. Andreev spectra and subgap bound states in multiband superconductors. *Phys. Rev. Lett.*, 103:077003, 2009.

[79] F. Romeo and R. Citro. Minimal model of point contact Andreev reflection spectroscopy of multiband superconductors. Preprint at arXiv:1407.7397v1 [cond-mat.supr-con], 2014.

[80] D. S. Inosov, J. T. Park, P. Bourges, D. L. Sun, Y. Sidis, A. Schneidewind, K. Hradil, D. Haug, C. T. Lin, B: Keimer, and V. Hinkov. Normal-state spin dynamics and temperature-dependent spin-resonance energy in optimally doped $BaFe_{1.85}Co_{0.15}As_2$. *Nature Phys.*, 6:178–81, 2010.

[81] Yu. G. Naidyuk, O. E. Kvitnitskaya, N. V. Gamayunova, L. Boeri, S. Aswartham, S. Wurmehl, B. Büchner, D.V. Efremov, G. Fuchs, and S.-L. Drechsler. Single 20meV boson mode in Kfe_2As_2 detected by point-contact spectroscopy. Preprint at arXiv: 1408.1509v1 [cond-mat.supr-con], 2014.

[82] H. Z. Arham and L. H. Greene. Point contact spectroscopy of Fe pnictides and chalcogenides in the normal state. *Curr. Opin. Solid St. M.*, 17:81, 2013.

[83] W.-C. Lee, W. K. Park, H. Z. Arham, L. H. Greene, and P. W. Phillips. Theory of Point Contact Spectroscopy in Correlated Materials. Preprint at arXiv:1405.6357 [cond-mat.str-el], 2014.

[84] R. S. Gonnelli, D. Daghero, D. Delaude, M. Tortello, G. A. Ummarino, V. A. Stepanov, J. S. Kim, R. K. Kremer, A. Sanna, G. Profeta, and S. Massidda. Evidence for gap anisotropy in CaC_6 from directional point-contact spectroscopy. Phys. Rev. Lett., 100:207004, 2008.

[85] A. A. Golubov and I. I. Mazin. Designing phase-sensitive tests for Fe-based superconductors. Appl. Phys. Lett., 102:032601, 2013.

IntechOpen